



UNIVERSITÄT BAYREUTH

Abt. Mikrometeorologie

**The OP-2 open path infrared gas analyser
for CO₂ and H₂O**

Gesa M. Herold

Christoph Thomas

Thomas Foken

Arbeitsergebnisse

Nr. 27

Bayreuth, Januar 2005

Die Arbeit wurde durch Frau Herold im SS 2004 im Rahmen des Forschungspraktikums Mikrometeorologie angefertigt. Die Betreuung erfolgte durch Dipl.-Geoökol. Christoph Thomas und Prof. Dr. Thomas Foken. Die Untersuchungen erfolgten in Abstimmung mit der Firma ADC BioScientific, Herts, U.K.

Arbeitsergebnisse, Universität Bayreuth, Abt. Mikrometeorologie, Print, ISSN 1614-8916
Arbeitsergebnisse, Universität Bayreuth, Abt. Mikrometeorologie, Internet, ISSN 1614-8924
<http://www.bayceer.uni-bayreuth.de/mm/>

Eigenverlag: Universität Bayreuth, Abt. Mikrometeorologie
Vervielfältigung: Druckerei der Universität Bayreuth
Herausgeber: Prof. Dr. Thomas Foken

Universität Bayreuth, Abteilung Mikrometeorologie
D-95440 Bayreuth

Die Verantwortung über den Inhalt liegt beim Autor.

1. Introduction

Open path fast response gas analysers have been used for simultaneous fast response measurements of carbon dioxide (CO₂) and water vapour (H₂O) in the atmosphere for a long time. The principle of operation is based on the attenuation of certain infrared or ultraviolet radiation bands by CO₂ or water vapour molecules. Optical measurements provide direct analysis of gas concentrations in the turbulent flow with high resolution in time and space. Combined with a sonic anemometer, they are convenient instruments for the measurement of turbulent CO₂ and latent heat fluxes, as they encompass the complete turbulence spectrum including the inertial subrange and therefore meet the requirements for the eddy covariance method (Lee, 2004). The growing interest in simultaneous flux measurements of CO₂ and water vapour for research of greenhouse gas sequestration as well as for plant physiological studies increases the need of exact measuring devices.

The first optical open path instruments for direct measurements in the atmosphere were restricted to the analysis of water vapour concentration. Water vapour absorbs both in the ultraviolet (UV) and in the near infrared (IR). However, absorption in the IR spectral range is poorer and requires longer optical path lengths (Heikinheimo *et al.*, 1989). For gases with higher partial densities such as H₂O and CO₂, the IR absorption is appropriate though (Foken *et al.*, 1995).

First attempts at optical measurements of humidity fluctuations were made employing bands in the near infrared (Elagina 1962). An elongated folded optical path of several meters length caused problems with the optical alignment though, making the measurements unsound. Chen and Mitsua (1967) report on a portable type of hygrometer. One of the first open path hygrometers functioning in the far UV was the Lyman-alpha hygrometer (Krečmer and Karpovič, 1973, Martini *et al.* 1973, Buck 1976, 1985). This device uses the Lyman-alpha emission line of atomic hydrogen (121.56 nm), which is strongly absorbed by water vapour. Its performance includes a response time of a few milliseconds, compact size with a path length of a few centimetres and a sensitivity over a range of -80° to 40°C. Restrictions of the instrument are the limited lifetime of the hydrogen source due to loss of hydrogen from the source, and window deterioration causing drifts of the instrument output (Heikinheimo *et al.*, 1989) as well as continual drift in calibration and sensitivity (Lind and Shaw, 1991). Campbell and Tanner (1985) developed an UV open path

hygrometer using a krypton source with emission wavelengths of 116.49 nm and 123.58 nm. The source offers an increased lamp life and better stability than the Lyman-alpha source. Oxygen absorption interferes with water vapour absorption in the krypton emission lines and has to be accounted for. A listing of commercially available UV and IR hygrometers can be found in Foken (2003).

The first open path CO₂ sensors used for micrometeorological studies came up in the late 1970s (Bingham *et al.* 1978, Brach *et al.* 1981). Only shortly after, instruments for simultaneous measurements of CO₂ and H₂O were developed. The basic operation principle is the same, whereas their configuration differs from the implements described above. For the two different gases of interest, different absorption bands must be used, in general close to 4.3 μm and 2.6 μm for CO₂ and H₂O, respectively. Usually, narrow band-pass interference filters of different centre wavelengths mounted on a chopper wheel are placed in front of the detector, including an additional reference filter near 3.9 μm where neither CO₂ nor H₂O absorbs and an opaque filter. The dark value is subtracted from the other measurements, and the CO₂ and H₂O signals are divided by the reference signal (Ohtaki and Matsui, 1982), compensating for instability caused by background emission, dust in the pathway or electrical drift (Heikinheimo *et al.*, 1989). The requirements are a broadband source emitting all wavelengths of interest and a detector sensitive for all wavelengths. Lead selenide (PbSe) and mercury cadmium telluride (HgCdTe) detectors are commonly used. The optical path can be unfolded or folded. In the unfolded design, the source and the detector are situated in individual housings at opposite ends of the device. This geometry reduces flow distortion due to smaller sized probe head. On the other hand, equal drifts of the source temperature and detector temperature have an opposite effect on the signal output and can compensate each other (Heikinheimo *et al.*, 1989). In different housings the temperature drifts of source and detector can differ, causing low frequency drift of the output signal. In the folded path design, one or more mirrors reflect the beam from the source to the detector. The folded optical path allows a smaller physical path length leading to a higher frequency response. Additionally, a longer optical path results in higher sensitivity while the sampling volume stays small. The source needs to be adequately intensive for the longer folded path.

Simultaneous measurements of CO₂ and H₂O employing a multiple beam infrared absorption gas analyser were first conducted by Ohtaki and Matsui (1982).

They used a broadband nichrome filament source and chose an optical path length of 20 cm in agreement with the span length of the sonic anemometer used in the study. The high rotation speed of the chopper wheel provides nearly simultaneous measurements of CO₂, H₂O, the reference value and a dark level. Major problems were drift of the source's peak wavelength and excessive heat produced by the source, as well as low frequency drift due to modulating filter and source temperatures (Green and Kohsiek, 1995).

Most later devices differed from this basic design only in details such as source type, choice of absorption bands, rotation speed of the chopper wheel, lens type or optical path length and physical configuration. Heikinheimo *et al.* (1989) report on a miniature CO₂ and water vapour sensor with a once folded absorption path of 12.5 cm length and absorption bands for CO₂ and H₂O of 4.26 µm and 2.60 µm, respectively. The small design features reduced flow distortion. Cerni (1994) doubts the sensor's stability due to high scatter in the output, though. Auble and Meyers (1992) developed a combined infrared CO₂ and H₂O gas analyser with a four times folded path of 80 cm length and a physical path of 20 cm. They selected absorption bands of 2.61 µm, 4.22 µm, and 3.91 µm for water vapour, CO₂ and the reference band, respectively. While the noise level of H₂O was found to contribute only little to variance, the noise in the CO₂ signal was significant. Power spectral densities for CO₂ and water vapour exhibited the -5/3 law by Kolmogorov (1941) at frequencies higher than 0.1 Hz. Problems with instability were caused by source temperature modulation.

In order to obtain more accurate measurements, further improvements of the measuring devices must be achieved. In this study, the performance of the new OP-2 infrared open path gas analyser (ADC BioScientific, Herts, Great Britain) with respect to absolute concentrations of CO₂ and water vapour, to the CO₂ flux and the latent heat flux was investigated. The configuration of the device with a folded path of 80 cm and a physical path of 20 cm is particularly similar to the implement described by Auble and Meyers (1992). The measurements were conducted from July 6th till August 8th, 2004, at the Waldstein site, Fichtelgebirge Mountains, Germany. As a reference instrument, a LI-7500 gas analyser (LI-COR Inc., Lincoln, Nebraska, USA) with unfolded path configuration was used.

2. Theory

2.1. Gas density measurement

Radiant energy is absorbed by atmospheric gases at specific wavelengths. According to Beer's law, the attenuation of monochromatic radiation by a single absorption gas can be related to the concentration of the absorbent:

$$I_{\lambda} = I_{0\lambda} \cdot \exp\left(-k_{\lambda} \cdot d \cdot \frac{c}{c_0}\right) \quad (1)$$

where I_{λ} is the detected intensity at wavelength λ , $I_{0\lambda}$ the intensity at absorption concentration c_0 and wavelength λ , k_{λ} the absorption coefficient at wavelength λ of the absorbing gas, d the length of optical path and c the concentration of the absorbing gas.

As source intensity and detector response may drift with temperature changes, and dust in the optical path may cause scattering and absorption of radiant energy, normalizing the signal with a non-absorbing reference signal is reasonable. According to Auble and Meyers (1992), both effects may be combined in an attenuation factor A . In the reference band, the absorption coefficient of the gas to be measured is close to zero. Thus, equation (1) becomes

$$I_{\lambda} = A \cdot I_{0\lambda} \cdot \exp\left(-k_{\lambda} \cdot d \cdot \frac{c}{c_0}\right) \quad (2)$$

for the general case and

$$I_{\lambda r} = A \cdot I_{0\lambda r} \quad (3)$$

for the reference wavelength where $I_{\lambda r}$ and $I_{0\lambda r}$ are the detected intensity and the intensity at absorption concentration c_0 at reference wavelength, respectively. After normalizing with equation (3), equation (2) becomes

$$\frac{I_{\lambda}}{I_{\lambda r}} = \frac{I_{0\lambda}}{I_{0\lambda r}} \cdot \exp(-k_{\lambda} \cdot \rho \cdot d) \quad (4)$$

where the effect of A is eliminated.

The application of Beer's law in open path measurements of gas concentration is not exact, since the absorption bands consist of several wavelengths with different absorption coefficients. In addition, CO_2 and water vapour are not the only gases that

absorb in the IR bands chosen for gas concentration measurements. The contribution of other gases to the attenuation at the chosen wavelength is little, but has to be accounted for. Therefore, equation (1) becomes

$$I = \sum_{i=1}^m I_{0\lambda_i} \cdot \exp\left(-\sum_{j=1}^n k_{\lambda_{ij}} \cdot \rho_j \cdot d\right) \quad (5)$$

where i is the index for i th wavelength and j the index for j th absorption gas.

Since equation (5) is rather complex, an empirical polynomial calibration function between a known gas concentration and voltage output as an approximate measurement of I is preferable.

2.2. Flux measurement

The eddy covariance method provides direct measurements of vertical turbulent fluxes, such as the latent and the sensible heat flux, the flux of CO₂ and momentum flux. Atmospheric exchange is organized in eddies of different sizes



Figure 1: Scheme of the Reynolds decomposition for variable x . (Foken, 2003)

which are represented by the fluctuation of a signal. The net vertical scalar flux is the difference between upward and downward moving eddies and its transported constituents. The eddy covariance method is based on the Reynolds decomposition, which splits the instantaneous measurement in a mean and a fluctuating part (Figure 1).

With the Reynolds' postulates, the covariance of the vertical wind component and the scalar quantity is defined as

$$\overline{w'\xi'} = \frac{1}{N-1} \sum_{i=1}^{N-1} (\overline{w} - w')(\overline{\xi} - \xi') \quad (6)$$

where bars and primes represent mean values and fluctuating values, respectively, w is the vertical wind component and ξ the scalar quantity. It is a direct measurement of the flux. The latent heat flux Q_E is given by

$$Q_E = \rho \cdot \lambda \cdot \overline{w'q'} = \lambda \cdot \overline{w'a'} \quad (7)$$

where ρ is the density of air, λ the evaporation enthalpy of water, q the specific humidity in g water vapour per g moist air and a the absolute humidity in g m⁻³. The CO₂-flux F_c is given by

$$F_c = \rho \cdot \overline{w'c'} \quad (8)$$

where ρ is the density of air and c the concentration of CO₂.

The eddy covariance method is derived from simplifying assumptions such as stationary conditions, horizontally homogeneity of the terrain and disappearance of the mean vertical wind. A list of applied simplification can be found in Foken and Wichura (1996). Deviations from these prerequisites have to be accounted for. Therefore, a series of corrections and transformations has to be applied to the measurements and the quality of the data has to be controlled.

Usually, the vertical wind does not disappear as the instrument causes upward movement of the air due to flow distortion. In addition, in inhomogenous terrain, vertical wind may go back to slopes. In order for the vertical wind velocity to disappear, the coordinate system needs to be rotated. The main axis is rotated into the mean wind direction and the tilt is corrected (Kaimal and Finnigan, 1994).

The spectral resolution of the measuring system is dependent on the time constant and the physical pathlength as well as on the sensor separation between the sonic anemometer and the gas analyser. A method for spectral correction in the short wave range via transmission functions is given by Moore (1986). However, the model spectra are based on data of the KANSAS (Kaimal and Wyngaard, 1990) experiment and may lack universality.

Webb et al. (1980) reported on the need of a density correction due to transport of water vapour and heat. The WPL correction converts volume related concentrations to mass related concentrations with respect to the density fluctuations and the humidity flow near the ground. When turbulent fluctuations are small in comparison to the mean concentrations, the correction is significant. For the CO₂ flux, the WPL correction can be as important as 50%, while the water vapour flux is only slightly varied (Liebethal and Foken, 2003; Liebethal and Foken, 2004).

All of the above corrections are incorporated in the TK2 software (Mauder and Foken, 2004) used in this study. Additional features of the TK2 are the conversion of the buoyancy flux to the sensible heat flux by Schotanus (1983), and a despiking procedure to remove erroneous values.

The quality of eddy covariance data depends on stationarity and on the development of turbulence. Therefore, Foken and Wichura (1996) recommend a classification of data quality according to a stationarity test and a turbulence characteristics test. If the sonic anemometer that is used is not omnidirectional, an additional test on the sector of wind direction is necessary. The stationarity test compares the mean of a time series of thirty minutes to the mean of shorter intervals. The rating of the time series' stationarity is based on the deviation. In the turbulence characteristics test, the measured characteristics are compared to a theoretical value of the characteristics according to the stability of stratification and friction velocity (Foken *et al.* 1991, Thomas und Foken, 2002). The data are rated in 3 quality classes with respect to the tests, quality class 0 representing best quality. The quality assessment is also integrated in the TK2 software.

3. OP-2 sensor design

The OP-2 open path gas analyser (ADC BioScientific, Herts, Great Britain) is a fast response multiple beam infrared sensor designed for simultaneous measurement of the fluctuations of carbon dioxide (CO₂) and water vapour (H₂O) in the atmosphere. The system includes the sensor itself, a power supply box and interconnecting cables. A calibration hood is also supplied. The chassis consists of anodised aluminum. The probe head has a cylindrical shape and is relatively large with a length of 37 cm and a diameter of 7.6 cm. The sensor's electronics are housed in the rear end of the probe head. They are sealed with a cover sleeve and nitrile 'O' rings.

A scheme of the geometrical arrangement of the OP-2 sensor is shown in Figure 2. The 12 V DC source emits broadband radiation, which is collimated with a calcium fluoride (CaF₂) lens and passes through a weather-sealed abrasion resistant sapphire window into the absorption path. The optical path is folded by means of two coated weather resistant mirrors, a spherical and a plane one, resulting in a four

times folded path of 80 cm length, whereas the physical path is 20 cm. The longer optical path provides increased sensitivity of the sensor. The material of the mirrors

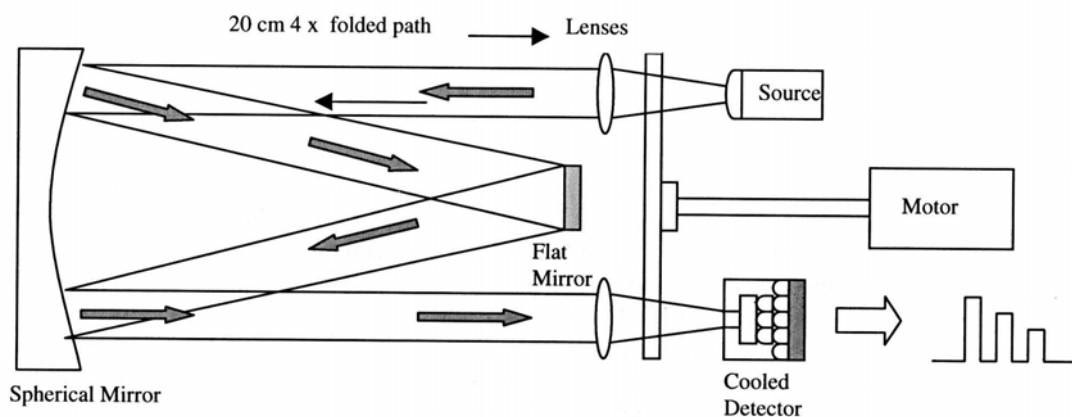


Figure 2: Basic geometry of the OP-2 open path gas analyser (Instruction Manual)

was not specified by the manufacturer. A second sapphire window and a second CaF_2 lens are placed at the end of the optical path. A chopper wheel with three narrow-bandpass interference filters is positioned in front of the detector. The centre wavelengths of the filters are $2.6 \mu\text{m}$, $4.3 \mu\text{m}$ and $3.9 \mu\text{m}$ for H_2O , CO_2 and the reference value, respectively. The IR radiation that passes the filters is focused on the active surface of the lead selenide (PbSe) detector with precise thermoelectrical cooling. The detector's maximum sensitivity is reached in the $2 \mu\text{m}$ to $5 \mu\text{m}$ wavelength band. The thermoelectrical cooling increases the sensitivity of the detector and minimizes temperature related low frequency drift.

The chopper wheel rotates with 3000 revolutions per minute, providing an instrument response of 50 Hz. During each revolution, a dark and a light value for each filter are measured. Therefore, the microprocessor-controlled sampling circuitry measures the detector response six times per revolution. The dark values are subtracted from the light values, and the CO_2 and the H_2O signals are normalized with the reference value. Thus, dust accumulation and fluctuation of the source strength are accounted for. In addition, the internal temperature is measured by means of an integrated circuit temperature sensor and stored. The signals are fed to a temperature compensation circuitry in the power supply box. In further circuitry, the independent adjustment of signal gains and offsets for both CO_2 and H_2O are possible. The basic response of 50 Hz is filtered to a 15 Hz output signal.

The output signals are constant analog voltages referring to the concentrations of CO₂ and H₂O. A shielded signal cable for the data acquisition is supplied.

An exact description of the mode of operation and instructions for installation can be found in the instruction manual.

4. Instrument performance

4.1. Calibration

For the calibration of carbon dioxide and water vapour concentrations, a calibration hood is placed between the sapphire windows. For the calibration of the CO₂ response, several calibration gases of known CO₂ concentration are directed through the optical path at a constant flow. The calibration of water vapour response measurements is more sophisticated. An air stream is led over a pan of boiling water which causes saturation of the air. This moist air is blended with dry air, and the resulting moisture is controlled with a dew point analyser. The stream of blended air is then led through the optical path. OP-2 calibration was conducted by ADC.

In the instruction manual, a linear least squares fit is recommended for the CO₂ calibration curve, while the water vapour concentration, which varies more widely, is supposed to be fit to a second degree polynomial. However, for the complete range of calibration values these recommendations were found unsound. Although the correlations of the recommended curves were above 0.9, the sum of quadratic errors showed a poor precision of the linear and the second degree polynomial calibration for CO₂ and water vapour, respectively. The calibration curves provided by ADC were a fifth order polynomial function of the percentage of the total range of each concentration plotted against the percentage of total range of voltage output. Since these units are not suitable for most software, the data were converted to absolute concentrations in mmol m⁻³ and V for the concentration of the calibration gases and the signal output, respectively, assuming a temperature of 25 °C and a pressure of 1013 hPa. New calibration curves were calculated based on the converted data. The calibration curves for CO₂ and water vapour are shown in Figure 3 and Figure 4, respectively. The coefficients of the curves can be found in Table 1. The fifth degree polynomial fits for both CO₂ and water vapour met the

calibration concentrations very well with mean quadratic errors of $3.78 \cdot 10^{-3} \text{ mmol m}^{-3}$ for CO_2 and $7.16 \cdot 10^{-3} \text{ mmol m}^{-3}$ for H_2O . They are listed in Table 2.

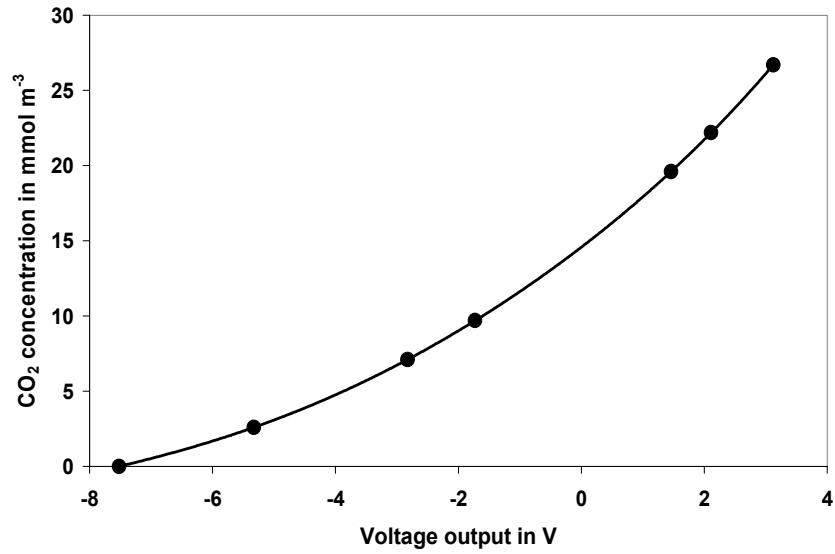


Figure 3: Fifth degree polynomial fit (line) to CO_2 calibration data (dots).

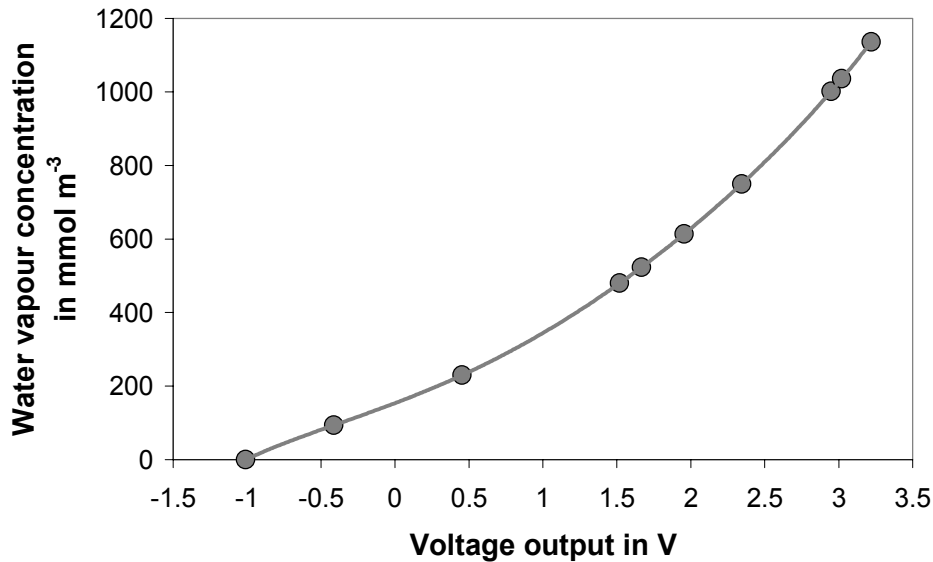


Figure 4: Fifth degree polynomial fit (line) to H_2O calibration data (dots).

Table 1: Coefficients (A_0 - A_5) and correlation coefficient of CO_2 and H_2O calibration curves. $\text{conc}_i [\text{mmol m}^{-3}] = A_0 + A_1 \cdot x + A_2 \cdot x^2 + A_3 \cdot x^3 + A_4 \cdot x^4 + A_5 \cdot x^5$ where conc_i represents the concentration of CO_2 or H_2O in mmol m^{-3} and x represents the signal output in V.

	A_0 [mmol m^{-3}]	A_1 [$\text{mmol m}^{-3} \text{V}^{-1}$]	A_2 [$\text{mmol m}^{-3} \text{V}^2$]	A_3 [$\text{mmol m}^{-3} \text{V}^3$]	A_4 [$\text{mmol m}^{-3} \text{V}^4$]	A_5 [$\text{mmol m}^{-3} \text{V}^5$]	R^2
CO_2 5 th degree polynomial	14.584	3.138	0.194	$9.6 \cdot 10^{-3}$	$1.3 \cdot 10^{-3}$	$9 \cdot 10^{-5}$	1
CO_2 linear	14.651	3.245	---	---	---	---	0.9988
H_2O 5 th degree polynomial	153.74	152.57	26.36	17.58	-6.971	1.098	1
H_2O linear	27.31	306.74	---	---	---	---	0.994

Table 2: Deviations of polynomial fits of CO₂ (a) and H₂O (b) from original concentration

a) voltage output	calibration gas concentration	concentration calculated with 5 th degree polynomial	quadratic error
V	mmol m ⁻³	mmol m ⁻³	mmol m ⁻³
-7.52	0	-0.16	2.48·10 ⁻²
-5.33	2.6	2.57	1.03·10 ⁻³
-2.83	7.1	7.11	5.61·10 ⁻⁵
-1.73	9.7	9.69	9.90·10 ⁻⁵
1.46	19.6	19.62	2.43·10 ⁻⁴
2.11	22.2	22.18	2.52·10 ⁻⁴
3.12	26.7	26.70	2.06·10 ⁻⁶
mean quadratic error			3.78·10 ⁻³

b) voltage output	calibration gas concentration	concentration calculated with 5 th degree polynomial	quadratic error
V	mmol m ⁻³	mmol m ⁻³	mmol m ⁻³
-1.01	0	0.01	1.37·10 ⁻⁴
-0.414	93.7	93.69	1.08·10 ⁻⁴
0.454	229.7	229.73	1.10·10 ⁻³
1.520	480.0	479.87	1.73·10 ⁻²
1.668	523.2	523.26	4.16·10 ⁻³
1.955	613.7	613.76	3.28·10 ⁻³
2.344	750.1	750.07	1.17·10 ⁻³
2.949	1001.6	1001.71	1.26·10 ⁻²
3.021	1036.0	1035.82	3.10·10 ⁻²
3.220	1136.1	1136.13	7.07·10 ⁻⁴
mean quadratic error			7.16·10 ⁻³

In most flux measurement software other than the TK2, the calibration routines require a linear calibration function. The use of a polynomial function is limited to more sophisticated software. Therefore, it was reasonable to linearise the calibration curve in segments. In this approach, we chose one segment for the CO₂ and the H₂O calibration each, in order to compare the signal outputs of the more exact polynomial calibration functions and the linear fit. The segments comprise the whole range of environmental concentrations that were expected during the measurements. Usual environmental concentrations of CO₂ are between 12.0 mmol m⁻³ and 18.0 mmol m⁻³, according to a span from 330 ppm to 450 ppm. The chosen segment of the calibration curve of H₂O covered the range between 320 mmol m⁻³ and 800 mmol m⁻³.

A direct linear fit to the calibration data was not possible for CO₂, as none of the calibration points provided were within the segment. Thus, a linear function was fit to calculated values of the fifth degree polynomial function mentioned above. In order to use the same approach for both gases, the linear fit for H₂O was calculated

using the same method. The linear fits of CO₂ and H₂O are shown in Figure 5. The linear calibration for CO₂ is in good agreement with the polynomial calibration function with a correlation coefficient of R²=0.9988. The deviations are greater for water vapour. This is due to the higher variability of atmospheric H₂O concentrations that have to be included in the considerations. The segment is therefore curved stronger than the polynomial segment of the CO₂ curve. The coefficients of the linear calibration functions of both gases are listed in Table 1.

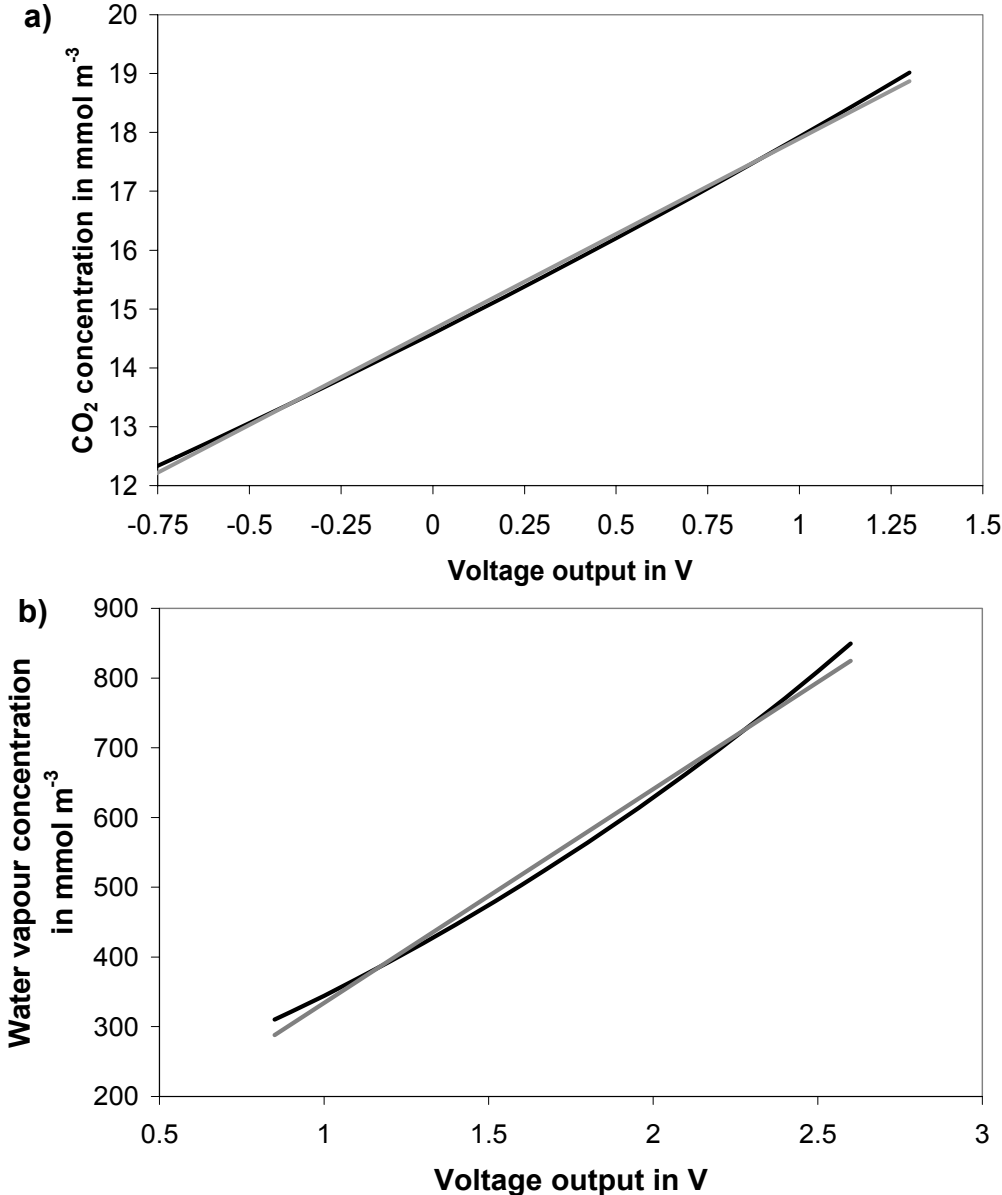


Figure 5: Linear function (grey) fit to a polynomial function (black) for CO₂ (a) and H₂O (b). The concentrations are in a range of 12 mmol m⁻³ to 18 mmol m⁻³ and of 320 mmol m⁻³ to 850 mmol m⁻³ for CO₂ and H₂O, respectively.

4.2. Field test

Field tests on the performance of the OP-2 gas analyser were conducted at the Fluxnet site Weidenbrunnen De-Wei, Fichtelgebirge mountains, Germany ($50^{\circ}08' N$, $11^{\circ}52'E$, 775 a. s. l.), over spruce forest (*Picea abies* L.) from July 6th, 2004 till August 8th, 2004. A detailed description of the site can be found in Gerstberger *et al.* (2004). The OP-2 was compared to a LI-7500 open path device (LI-COR Inc., Lincoln, Nebraska, USA) that is routinely used for long-term flux measurements and that was tested in international comparison studies (Oncley *et al.* 2002). A Solent R3-50 sonic anemometer (Gill Instruments Ltd.) was combined with the two gas analysers, in order to measure turbulent fluxes. Instrumentation was installed at 33.05 m above ground level, approximately 14 m above the canopy (canopy height $h_c = 19$ m). The direct distance between the gas analysers and the sonic anemometer was 33 cm. The data of both gas analysers were recorded by the analogue input channels of the sonic anemometer at a frequency of 20 Hz.

4.2.1. Data quality assessment

For the comparison of the performance of the OP-2 device with the LI-7500 gas analyser, half hour values were calculated for wind velocity, absolute humidity, concentration of CO₂, and for their variances and covariances. Only high quality data were used (cp. section 2.2.). Data of rainy and foggy periods were excluded from the comparison as droplets on the windows may affect the measurements of atmospheric CO₂ and water vapour. The same was done for half hour periods with relative humidity greater than 95% (measured with a reference instrument). Some half hour periods on rainy days were removed visually, as the data were clearly wrong and it could be supposed that the windows had not entirely dried off. Erroneous values of the variances of CO₂ and water vapour were a further motive for exclusion of data.

An additional source of flawed values was the limited voltage span that can be recorded by the sonic anemometer. The analogue input channels are constructed for incoming signals between 0 V and 5 V. Zero-crossings of the signal output in the 20 Hz time series and signals below 0 V seem to cause wrong values of the concentration. The axis intercept of the calibration function is given as the mean

concentration. For water vapour, the according values of the OP-2 data were 2.77 g m^{-3} (according to $153.65 \text{ mmol m}^{-3}$) with polynomial calibration and 0.49 g m^{-3} ($27.31 \text{ mmol m}^{-3}$) the linear approach. For CO_2 , the concentrations were $14.58 \text{ mmol m}^{-3}$ for the polynomial function and $14.65 \text{ mmol m}^{-3}$ in the linear case. The LI-7500 showed similar problems with the upper limit of 5 V , corresponding to 14.41 g m^{-3} (800 mmol m^{-3}) in the configuration in use. The phenomenon is demonstrated in Figure 6. The values were not considered in the comparison. Nevertheless, reconfiguration of the signal output span according to the analogue channels of standard sonic anemometers should be considered. Thus, the full range between 0 V and 5 V could be used as signals and a better resolution could be achieved.

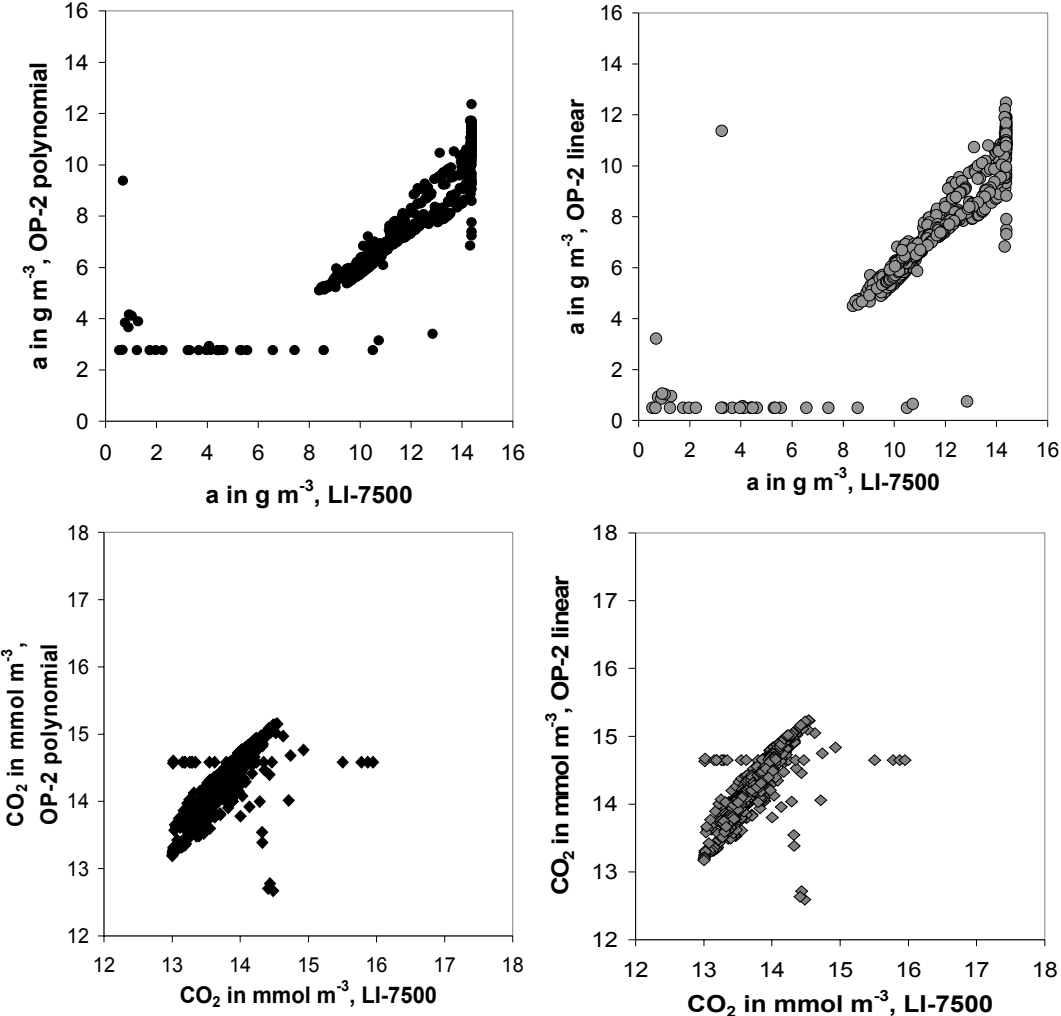


Figure 6: Scatter plots of the concentrations of water vapour (circles) and CO_2 (rhombuses) of the OP-2 with polynomial (black) and linear (grey) calibration functions plotted against the LI-7500 measurements. Constant values in the plots correspond to signal outputs $< 0 \text{ V}$ and $> 5 \text{ V}$.

4.2.2. Half hour means

The half hour values of CO₂ and the water vapour concentrations measured with the two gas analysers are shown in Figure 7 for the whole period of measurements. For the OP-2 device, only measurements based on the polynomial calibration are exhibited, because the linear calibration showed a similar pattern. The general shape of the OP-2 time series agrees with the measurements of the LI-7500. However, the absolute mean values of CO₂ and water vapour measured by the OP-2 gas analyser differ from those of the LI-7500.

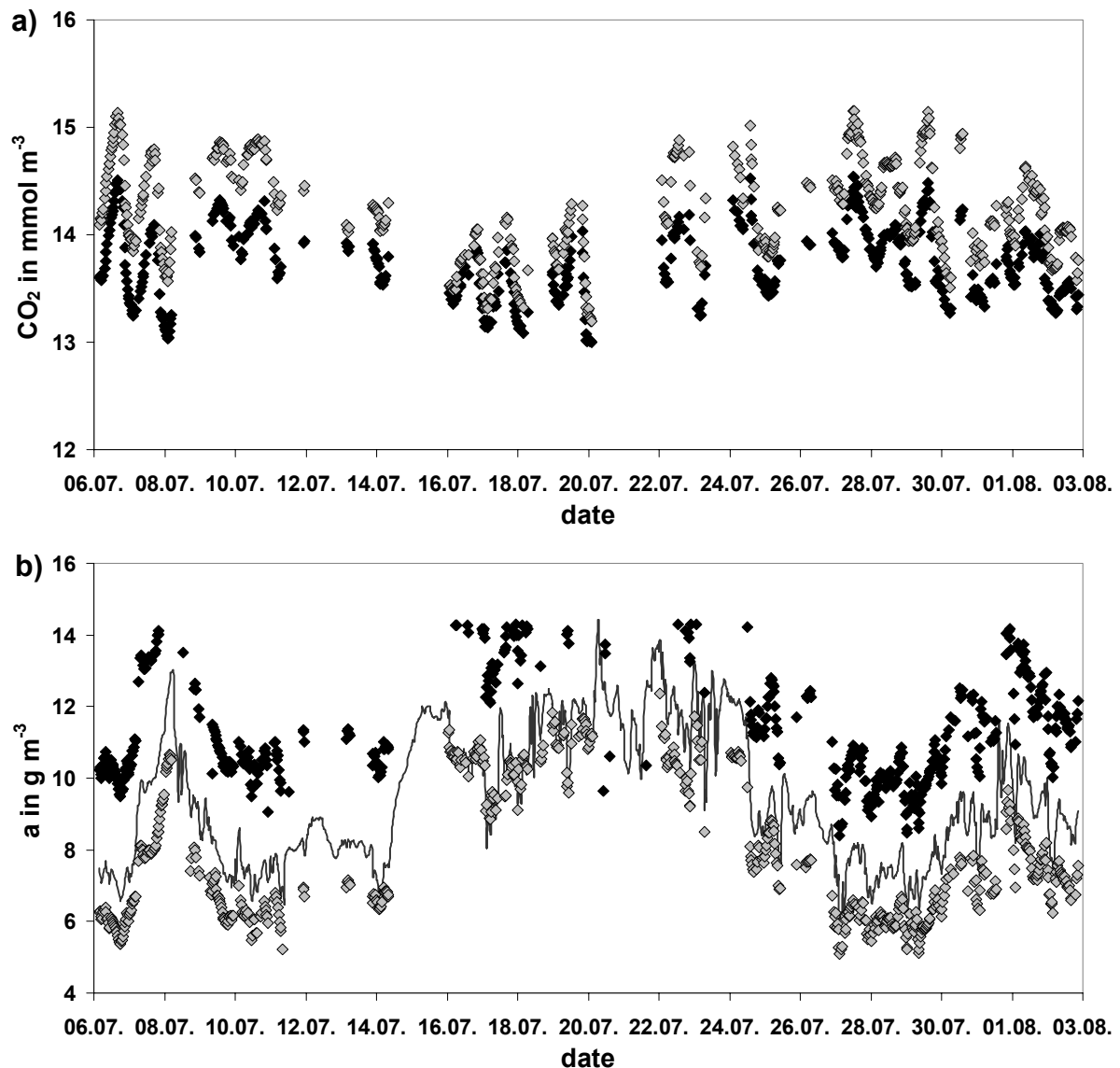


Figure 7: Measurements of CO₂ (a) and water vapour (b) concentrations of the LI-7500 (black) and of the OP-2 (grey) during the entire field test. The grey line in (b) shows an independent psychrometer measurement of the absolute humidity.

Figure 7(b) shows an additional independent measurement of the absolute humidity with a psychrometer (grey line). The LI-7500 had not been recalibrated for absolute values of humidity for several months due to the lack of a portable dew point hygrometer, causing a constant offset between the LI-7500 and the reference measure. The flux measurements are reliable, though, because they are not influenced by the offset of the absolute values. However, the absolute measurements of water vapour performed by the OP-2 were compared to both LI-7500 and the reference measurements. Recalibration of the LI-7500 for absolute values of CO₂ was performed only a short time before the field test.

In general, the OP-2 measured higher CO₂ concentrations than the LI-7500. Figure 8 shows a direct comparison of OP-2 data versus LI-7500 data with the same trend.

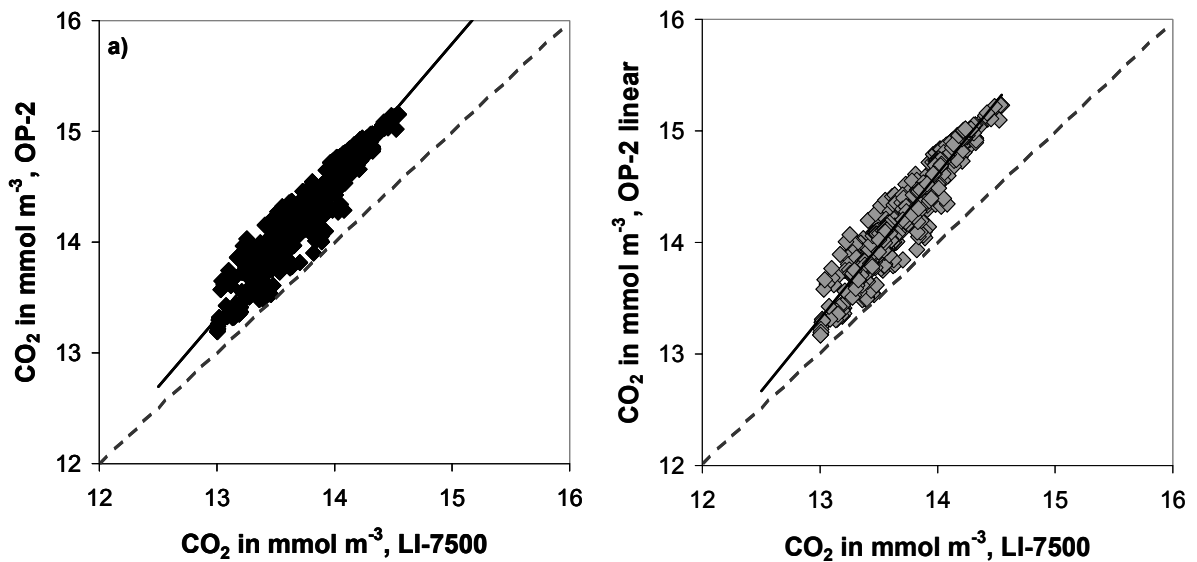


Figure 8: Scatter plot of the CO₂ data of the OP-2 with a) polynomial and b) linear calibration versus the LI-7500 data after quality control. The dashed line represents a slope of 1.

The correlation function between the OP-2 with polynomial calibration and the LI-7500 is

$$c_{op2pol} = 1.24 \cdot c_{LI-7500} - 2.8 \quad R^2 = 0.92 \quad (9)$$

where c_{op2pol} is the concentration of CO₂ calculated with the polynomial calibration function and $c_{LI-7500}$ is the concentration measured by the Li-COR device. The function for the linear approach is

$$c_{op2lin} = 1.30c_{LI-7500} - 3.58 \quad R^2 = 0.91 \quad (10)$$

where c_{op2lin} is the concentration of CO₂ calculated with the linear calibration function.

The slope of the correlation function is clearly greater than 1 for both calibrations. This observation does not correspond to the enhanced sensitivity for smaller concentration due to the longer optical path of the instrument because the overestimation is larger for high concentrations than for lower ones. There is no obvious association with calibration problems which would rather lead to a constant offset.

The performance of the OP-2 in water vapour measurements is entirely different. The OP-2 perspicuously underestimates the concentrations. Figure 9 exhibits the two scatter plots of the OP-2 measurements of water vapour concentration for both calibrations versus the data of the psychrometer.

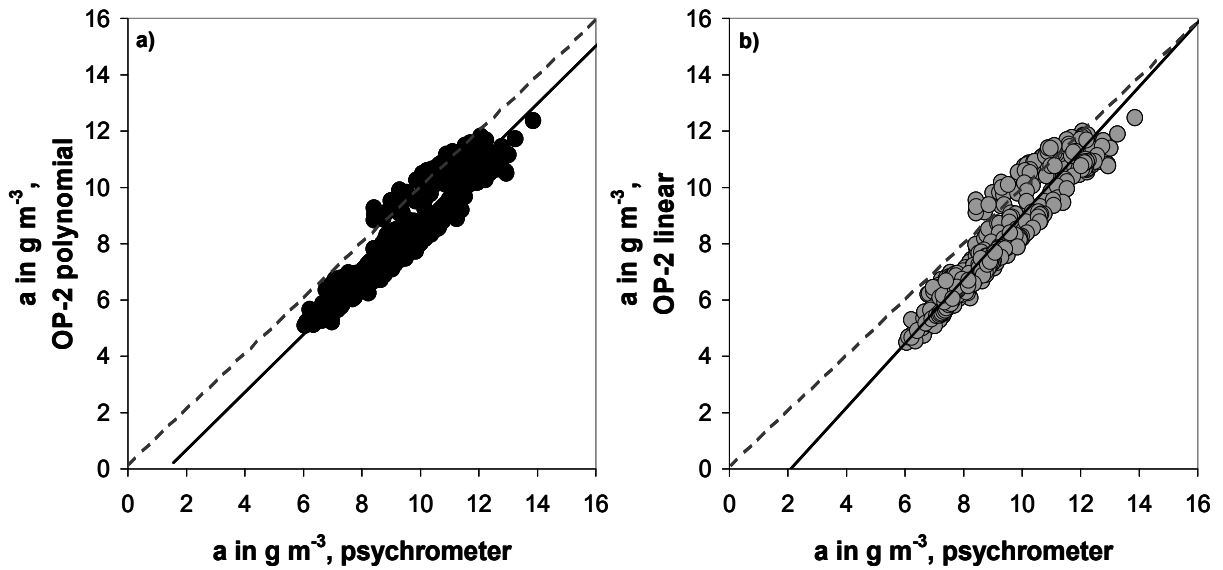


Figure 9: Scatter plot of the H₂O data of OP-2 with (a) polynomial, and (b) linear calibration versus a reference psychrometer after quality control. The dashed line represents a slope of 1.

The correlation functions are

$$a_{op2pol} = 1.02a_{ref} - 1.37 \quad R^2 = 0.90 \quad (11)$$

and

$$a_{op2lin} = 1.14a_{ref} - 2.38 \quad R^2 = 0.91 \quad (12)$$

for the polynomial and the linear calibration, respectively, where a is the absolute humidity in g m^{-3} . A calibration fault may be the reason for the underestimation. The slope in the polynomial approach is close to 1, so there is a constant offset of approximately 1.37 g m^{-3} between the OP-2 and the psychrometer. The comparison of the two gas analysers showed a slope of 0.98 when the linear calibration of the OP-2 was compared to the LI-7500 data. The rather large constant offset between the two instruments is due to the lack of recalibration described above combined with the effect of underestimation. Contrary to expectations, the agreement was better for the linear calibration. However, the LI-7500 was also calibrated with a linear function. Therefore, the linear approach for the OP-2 matches the LI-7500 calibration type. The polynomial calibration may still be more accurate as the comparison to the psychrometer confirms.

4.2.3. Variances

The variances of CO_2 and water vapour are different for the two instruments. In general, the variances of both gases are distinctly smaller for the OP-2 than for the LI-7500. In the scatter plots in Figure 10, the variances of the gas measurements performed by the OP-2 (linear) are compared to the variances of the LI-7500 concentrations. The regression for the polynomial calibration is not shown. The correlation functions and the correlation coefficients are given in Table 3.

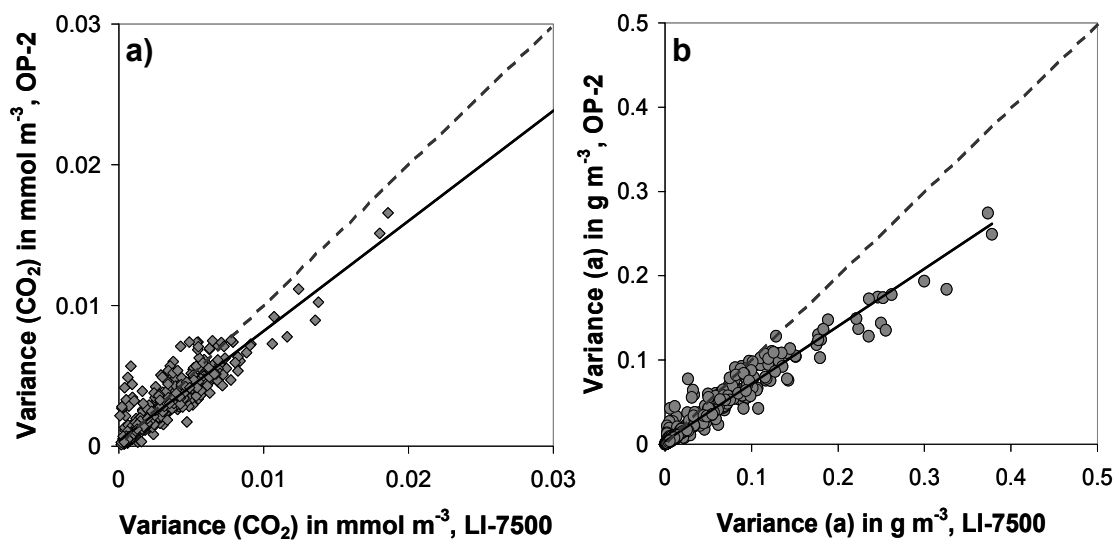


Figure 10: Scatter plots of the variances of the CO_2 (a) and water vapour concentrations (b) measured by the OP-2 (linear calibration) against variances measured by the LI-7500.

Table 3: Coefficients of the correlation functions between the variances measured by OP-2 and LI-7500. A_1 is the dimensionless slope, A_0 is the intercept (in mmol m^{-3} for CO_2 and g m^{-3} for water vapour).

		A_0	A_1	R^2
OP-2 linear vs. LI-7500	CO_2	0.0004	0.78	0.83
	H_2O	0.004	0.68	0.94
OP-2 polynomial vs. LI-7500	CO_2	0.0003	0.71	0.85
	H_2O	0.002	0.50	0.90

The slopes of all the correlation functions are far below 1, the biggest slope being 0.78. The scatter of the CO_2 variances is higher than for water vapour as the lower R^2 values reflect. The fluxes are therefore likely to be underestimated.

4.2.4. Comparison of flux measurements

The measurement of fluxes is the main field of application for the OP-2 gas analyser. Both OP-2 and LI-7500 were combined with the same sonic. It is therefore possible to directly compare the fluxes measured by the two devices. In Figure 11, the measurements of the latent heat flux and the flux of CO_2 performed by the OP-2 (linear approach) are plotted against the flux measurements of the LI-7500. The scatter is relatively small with R^2 values greater than 0.93 and 0.85 for the latent heat and the flux of CO_2 , respectively. Coefficients of the correlation function and correlation coefficients can be found in Table 4.

The scatter plot of the OP-2 with polynomial calibration compared to the LI-7500 is similar to Figure 11 though it shows smaller slopes and slightly higher scatter. The slopes of both the correlation function of the CO_2 flux and the latent heat flux stay below 0.87. For the CO_2 flux, the slopes are 0.71 and 0.76 for polynomial and for linear calibration, respectively. The OP-2 underestimates the magnitude of the flux of CO_2 , resulting in overestimation when the flux is negative and underestimation when it is positive with respect to the LI-7500 sensor. The latent heat flux is distinctly underestimated by the OP-2 sensor for large fluxes. For smaller fluxes, the underestimation is lower.

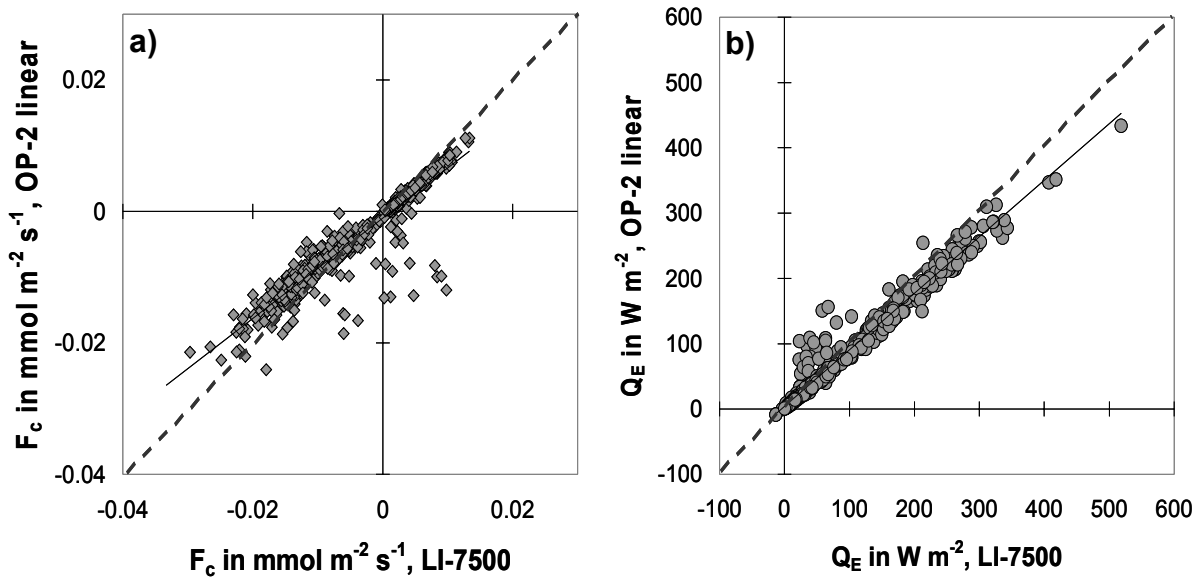


Figure 11: CO₂ flux (a) and latent heat flux (b) measurements of the OP-2 with linear calibration compared to the LI-7500 measurements. The dashed lines represent a slope of 1.

Table 4: Coefficients of the correlation functions of the latent heat flux (Q_E) and the CO₂ flux (F_C). A_1 is the dimensionless slope and A_0 the intercept (in $\text{mmol m}^{-2} \text{s}^{-1}$ for F_C and in W m^{-2} for Q_E).

		A_0	A_1	R^2
OP-2 linear vs. LI-7500	F_C	-0.001	0.763	0.87
	Q_E	3.90	0.866	0.97
OP-2 polynomial vs. LI-7500	F_C	-0.001	0.708	0.87
	Q_E	3.03	0.722	0.95

The underestimation of the fluxes can also be seen in the power spectra of CO₂ and water vapour and in the cospectra of the vertical wind component and the CO₂ or water vapour concentration. The power spectrum and the cospectrum of water vapour and CO₂ are shown in Figure 12 and Figure 13, respectively, for a sunny day at noon (7th July, 2004). The spectral energy densities were multiplied with the frequencies. Power spectra are normalised with the variance, while cospectra are not normalised. The OP-2 spectra and cospectra are marked with a grey line, the LI-7500 spectra are black.

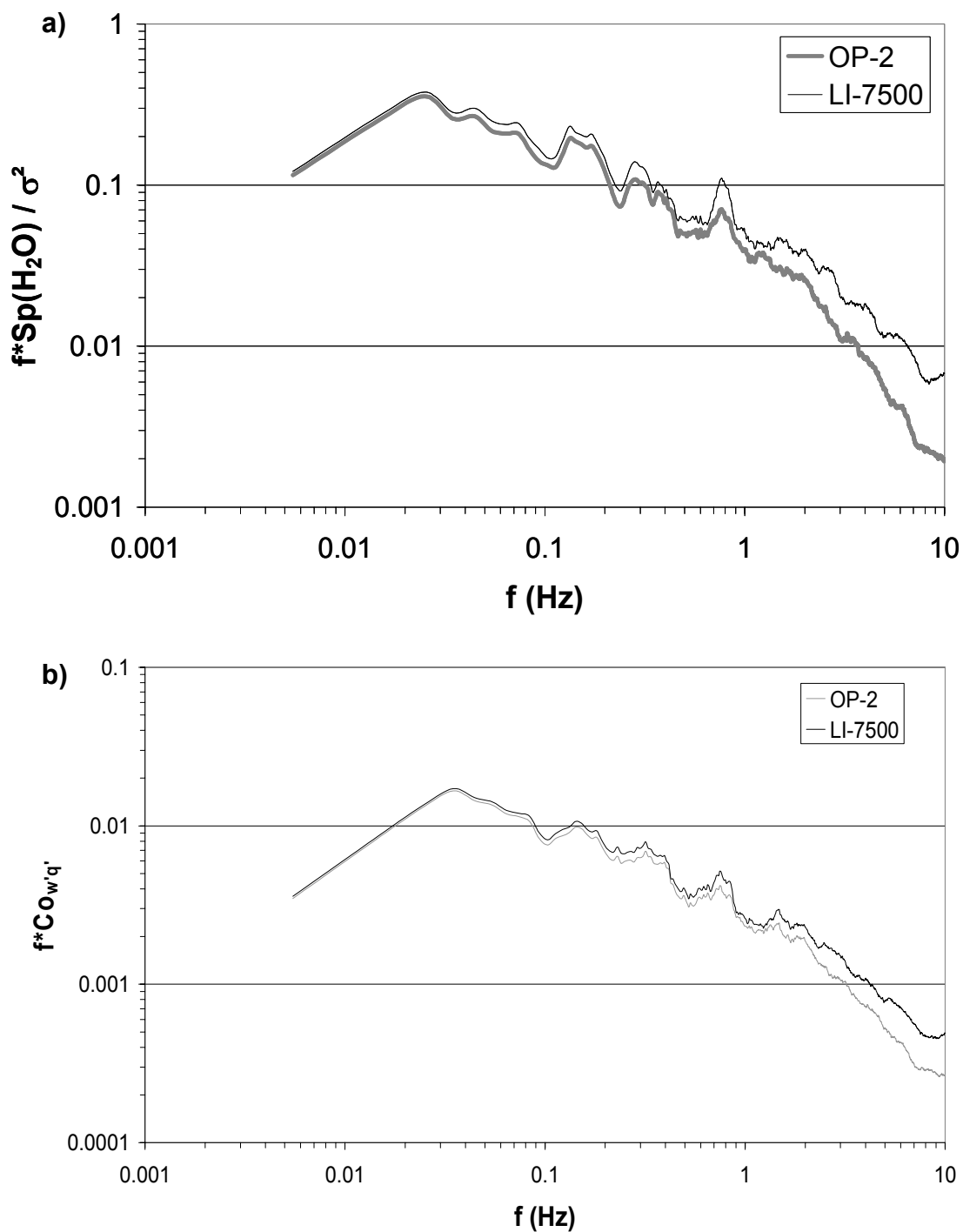


Figure 12: Power spectrum (normalized with variance) of water vapour concentration (a) and cospectrum (not normalized) of vertical wind and water vapour concentration at July 7th, 2004, 12:00h measured by the OP-2 (grey) and the LI-7500 (black) sensors.

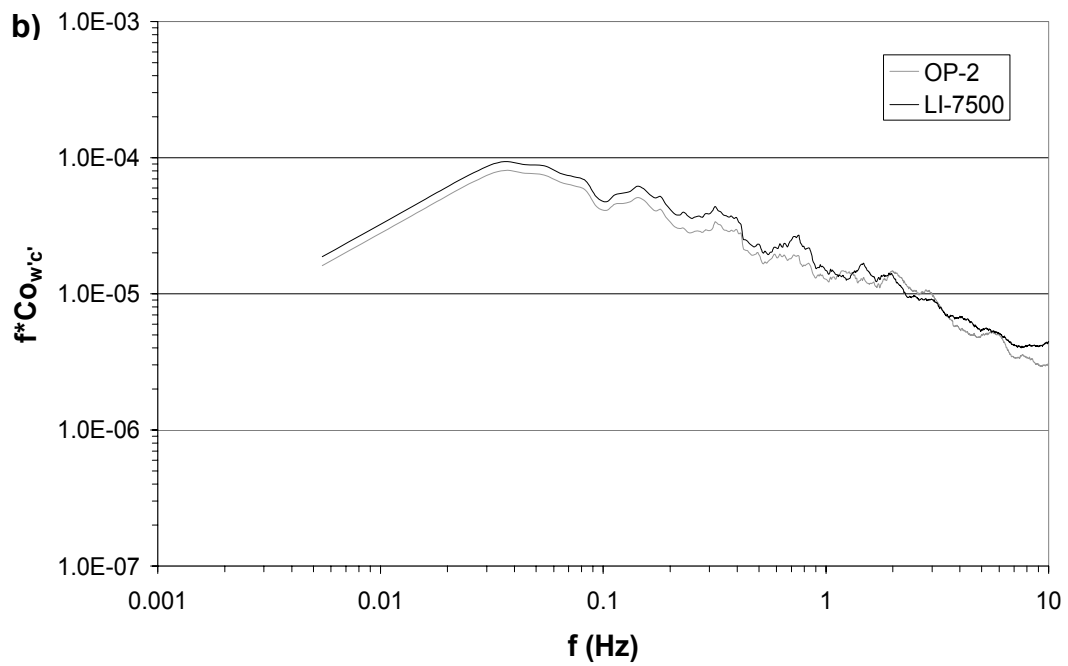
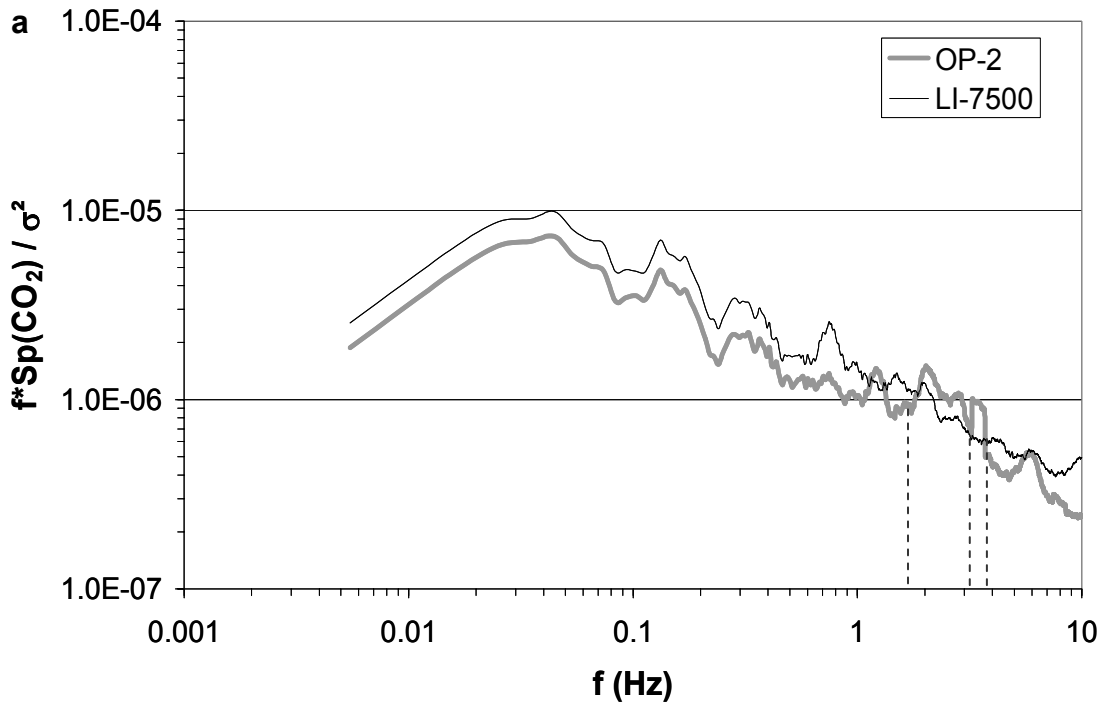


Figure 13: Power spectrum (normalized with variance) of CO₂ concentration (a) and cospectrum (not normalized) of vertical wind and CO₂ concentration at July 7th, 2004, 12:00h measured by the OP-2 (grey) and the LI-7500 (black) sensors.

The shape of the spectra and cospectra is similar for the two gas analysers. The energy spectrum of H₂O concentrations (Figure 12a) exhibits a very good agreement between the OP-2 and the LI-7500 measurements in low frequencies. However, for higher frequencies (inertial subrange), the slope of the OP-2 spectrum is steeper than the slope of the LI-7500 spectrum which leads to a slight underestimation of the high frequent contribution to the flux. The same tendency to a slight deviation can be found in the according cospectrum (Figure 12b).

For CO₂, the energy densities measured by the OP-2 are generally lower than the LI-7500 measurements. The power spectrum (Figure 13a) exhibits a small but distinct offset of the OP-2 in comparison with the LI-7500. Between approximately 1.8 Hz and 3.8 Hz, the power spectrum of the OP-2 shows a considerable deviation from the normal decline of the curve, pointed out with dashed lines in Figure 13a. The excursion between the second and the third dashed line (approximately between 3.1 Hz and 3.7 Hz) has a characteristic shape and can be found in most power spectra and cospectra of CO₂ concentration, especially during stable conditions of atmospheric stratification (during night). In nighttime spectra of water vapour concentration, the same excursion could be found, while there was no characteristic deviation during daylight hours. Figure 14 shows power spectra of water vapour concentration (a) and CO₂ concentration (b) at night (7th July, 2004, 00:30h). The chopper motor possibly initiates a slight oscillation of the device and the measured air column which may lead to additional noise at the frequency corresponding to the rotation speed of the chopper wheel. In stable stratification, the air stays within the optical path for a longer time and the oscillation affects the measurement to a higher degree. Another possible explanation for these high frequency deviations may be the sampling rate of the sonic anemometer of 20 Hz which differs from the 15 Hz output frequency of the OP-2 sensor. The highest frequency at which both devices meet is therefore 5 Hz (common denominator). This explanation does not account for the higher deviation of the CO₂ measurements than for water vapour or for the dependency on atmospheric stratification. Based on the observation height which is well above the canopy (1.74 zh_c⁻¹), we can exclude aliasing effects due to a too low output sampling frequency of 15 Hz. However, it is questionable if the initial sampling frequency of 50 Hz is appropriate for the relatively long physical path of 20 cm. Further investigation will be needed for the observed measurement artefacts.

Additional power spectra and cospectra can be found in Appendix I.

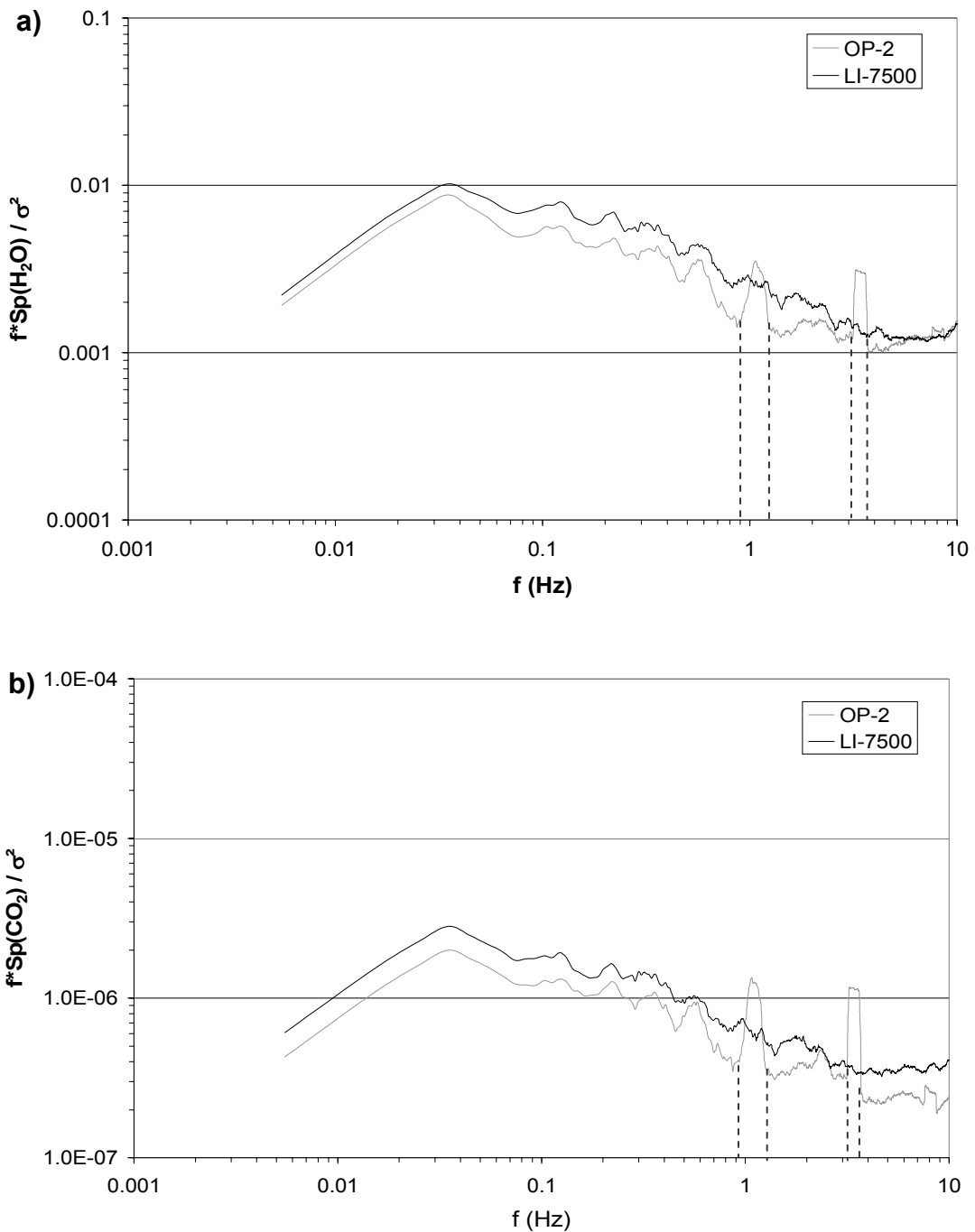


Figure 14: Power spectra (normalized with variance) of water vapour concentration (a) and CO₂ concentration (b) at 7th July, 2004, 00:30h. Considerable deviations from the relatively smooth curve are pointed out with dashed lines.

5. Conclusions

In this study, the performance of the new OP-2 open path gas analyser was compared to the performance of the LI-7500 open path device that is routinely used in long term measurements of the turbulent fluxes of latent heat and CO₂. The performance of the LI-7500 was tested in international experiments (Oncley et al. 2002, Beyrich, 2004). A higher sensitivity with respect to low concentrations of water vapour and CO₂ was expected from the OP-2 sensor due to the enhanced length of the optical path, whereas the resolution of turbulent fluctuations was expected to be lower. A systematic underestimation of turbulent fluctuations with increasing frequencies was observed in both single and co-spectra, which supports the hypothesis of lower resolution. The total range of OP-2 output voltage (-7.52 V to +3.12 V) was not in agreement with the range recorded by the sonic anemometer (0 V to 5 V). Therefore, low concentrations could not be measured and we could not find evidence of enhanced reliability of the OP-2 measurements in comparison with the LI-7500. In addition, adjustments of the instrument to standard anemometers used in micrometeorological studies might improve the quality of measurements.

Calibration of the OP-2 was done by ADC BioScientific, while the LI-7500 was calibrated at the University of Bayreuth. For CO₂ calibration, several standard gases with concentrations within the customary meteorological range (between 320 and 450 ppm) ought to be used which was not complied for the OP-2 calibration. The quality of CO₂ calibration may have suffered from the lack of calibration data in this range. CO₂ calibration of the LI-7500 was done a short time before the field test, whereas the H₂O calibration dated back over a longer period. Some offsets may have been caused by the different modes of calibration. Calibration against the same standard concentrations of CO₂ would be desirable. For the OP-2 sensor, a polynomial and a linear calibration function were compared. Linear calibration led to better agreement with the LI-7500. The reason may be the same type of calibration functions, as the LI-7500 also uses linear calibration.

The overall shape of the time series of mean values and fluxes was similar for both instruments. Mean values of the CO₂ concentrations for half hour intervals were higher for the OP-2 than for the LI-7500. The slope of a scatter plot of OP-2 data against data measured by the LI-7500 was significantly greater than 1. It is unlikely that calibration problems caused this overestimation. Neither does it reflect more

reliable measurements of low concentrations, as the overestimation increased with higher concentrations of CO₂. Half hour means of water vapour concentration were considerably underestimated by the OP-2. It should be verified if calibration problems caused the offset.

Variances of the OP-2 data were smaller than those of the LI-7500 for both H₂O and CO₂, implying an underestimation of fluxes. The differences of the absolute calibration of CO₂ are definitely not the reason for the underestimation of the variances. It is not certain if the same can be assumed for water vapour. Obviously, the spectral correction by Moore (1986) could not eliminate the discrepancy. It has to be confirmed in laboratory tests if the sampling rate of 15 Hz is equivalent to the time response of the device.

The flux measurements of both latent heat and CO₂ confirm the above assumption of underestimation, as the magnitudes of the CO₂ fluxes were considerably lower for the OP-2 than for the LI-7500. The underestimation was stronger for high frequent flux contributions as could be seen in the power and covariance spectra. In the power spectra of the OP-2, characteristic artefacts were found at high frequencies. They were stronger during nighttime conditions with stable stratification. The reason for the excursions in the spectra seems to be a technical problem. It must be checked at a laboratory scale. A possibility could be oscillation caused by the chopper motor. In addition, it should be considered that the OP-2 signal frequency (15 Hz) and the recording frequency of the analogue input channels of the Solent R3-50 sonic anemometer (20 Hz) were not the same which could cause spectral problems.

The OP-2 sensor showed an acceptable overall performance for flux measurements. For fundamental research, further improvement of the device is necessary, though.

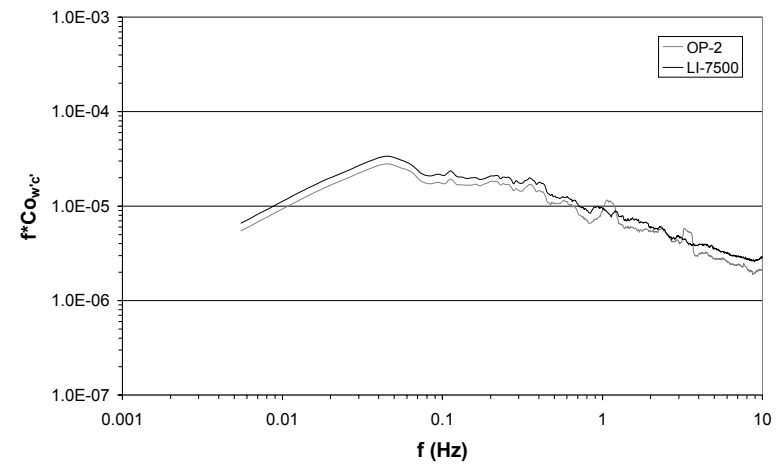
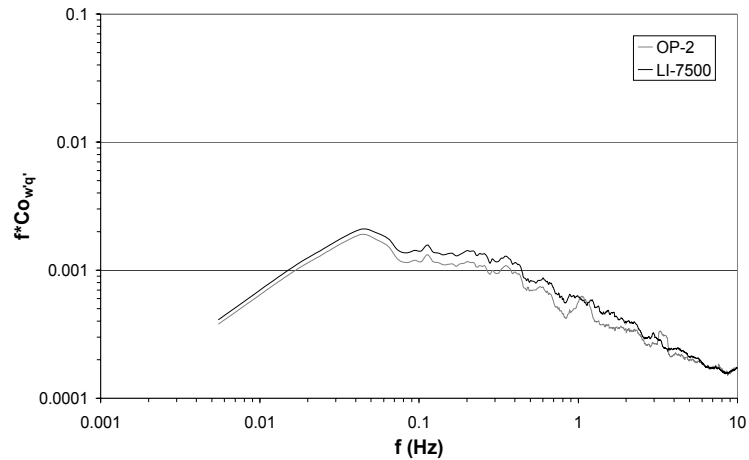
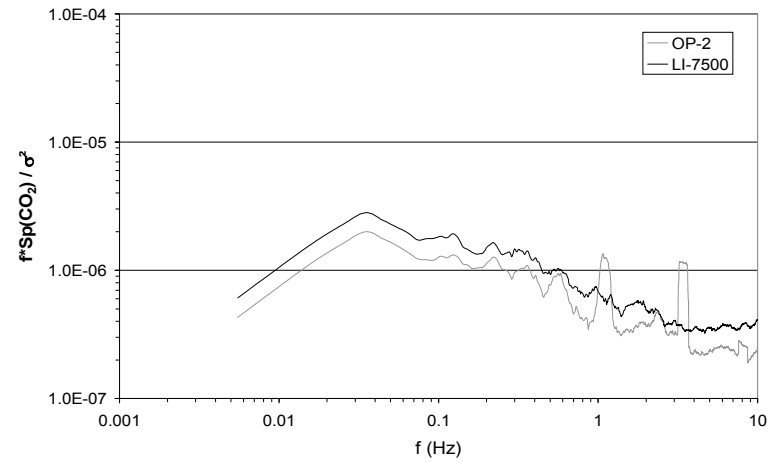
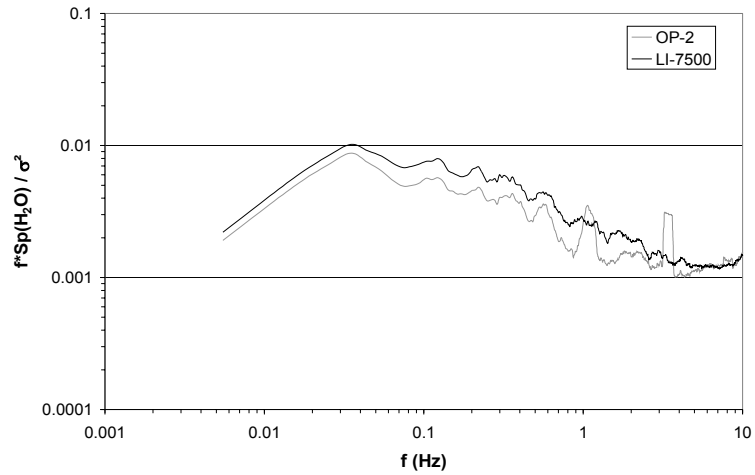
References:

- Auble, D. L. and Meyers, T. P., 1992: An open path, fast response infrared absorption gas analyser for H₂O and CO₂. *Boundary Layer Meteorology* **59**, 243-256.
- Beyrich, F. (Ed.), 2004: Verdunstung über einer heterogenen Landoberfläche – Das LITFASS – 2003 Experiment. *Deutscher Wetterdienst, Forschung und Entwicklung, Arbeitsergebnisse, ISSN 1430-0281*, 79, 100 pp.
- Bingham, G. E., Gillespie, C. H. and McQuaid, J. H., 1978: Development of a miniature, rapid response carbon dioxide sensor. *Lawrence Livermore Lab. Rep. UCRL-52330*, 18 pp.
- Brach, E. J., Desjardins, R. L. and St. Amour, G. T., 1981: Open path CO₂ analyzer. *J. Phys. E: Sci Instrum.* **14**, 1415-1419.
- Buck, A. L., 1976: The variable-path Lyman-alpha hygrometer and its operating characteristics. *Bull. Amer. Meteor. Soc.* **57**, 1113-1118.
- Buck, A. L., 1985: The Lyman-alpha absorption hygrometer. *Proceedings of the International Symposium Measurement and Control in Science and Industry, Washington D.C., ISA, Research Triangle Park*, 411-436.
- Campbell, G. S., and Tanner, B. D., 1985: A Krypton hygrometer for measurement of atmospheric water vapor concentration. *Proc. Int. Symposium Measurement and Control in Science and Industry, Washington D.C., ISA, Research Triangle Park*, 609-612.
- Cerni, T. A., 1994: An infrared hygrometer for atmospheric research and routine monitoring. *J. Atmos. Oceanic Technol.* **11**(2), 445-462.
- Chen, H. S., and Mitsua Y., 1967: An infrared absorption hygrometer and its application to the study of the water vapor flux near the ground. *Special contributions Geophysical Institute, Kyoto Univ.* **7**, 83-94.
- Elagina, L. G., 1962: Optičeskij pribor dlja izmerenija turbulentnych pul'sacii vlažnosti. *Izv. AN SSSR, sre. geofiz.* 1100-1107.
- Foken, T., Dlugi R. and Kramm G., 1995: On the determination of dry deposition and emission of gaseous compounds at the biosphere-atmosphere interface. *Meteorol. Zeitschrift, N.F.* **4**, 91-118.

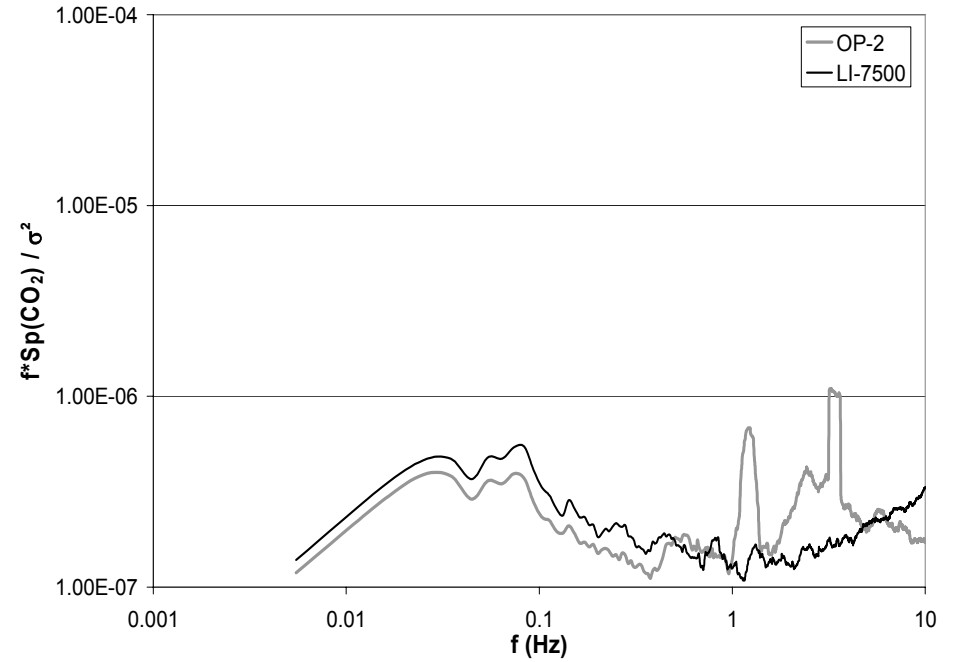
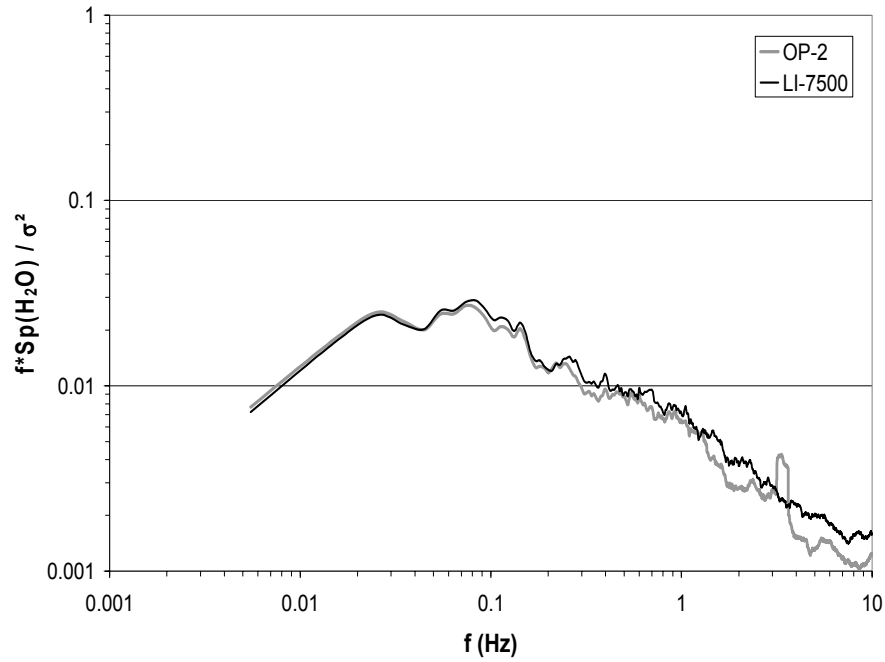
- Foken, T., Skeib, G., Richter, S. H., 1991: Dependence of the integral turbulence characteristics of the stability of stratification and their use for Doppler-Sodar measurements. *Z Meteorol* **41**, 311-315.
- Foken, T. and Wichura, B., 1996: Tools for quality assessment of surface-based flux measurements. *Agric Forest Meteorol* **78**: 83-105
- Foken, T., 2003: *Angewandte Meteorologie, Mikrometeorologische Methoden*. Springer, Heidelberg, 289 pp.
- Foken, T., Goeckede, M., Mauder, M., Mahrt, L., Amiro, B. D., Munger, J. W. (2004): Post-field data quality control. in Lee X., Massman W., Law B.: *Handbook of Micrometeorology: A Guide for Surface Flux Measurement and Analysis*, Kluwer, Dordrecht 181-208 (2004).
- Gerstberger, P., Foken, T., Kalbitz, K., 2004: The Lehstenbach andn Steinkreuz catchments in NE Bavaria, Germany. In: Matzner (ed.): *Biogeochemistry of forested catchments in a changing environment: Ecological Studies*. Springer, Heidelberg **172**, 15-41.
- Green, A. E. and Kohsiek W., 1995: A fast response, open path, infrared hygrometer, using a semiconductor source. *Boundary Layer Meteorology* **74**, 353-370.
- Heikinheimo, M. J., Thurtell G. W., and Kidd G. E., 1989: An open path fast response IR spectrometer for simultaneous detection of CO₂ and water vapor fluctuations. *Journal of Atmospheric and Oceanic Technology* **6**, 624-636.
- Kaimal, J. C. and Finnigan, J. J., 1994: *Atmospheric boundary layer flows: Their structure and measurement*. Oxford University Press, New York, NY, 289pp.
- Kaimal, J. C., Wyngaard, J. C., 1990: The Kansas and Minnesota experiments. *Boundary-Layer Meteorol.*, **50**, 31-47.
- Kolmogorov, A. N., 1941: Rassejanie energii pri lokalno-isotropoi turbulentnosti. Dokl AN SSSR **32**, 22-24.
- Krečmer, S.I. and Karpovič, J.V., 1973: Maloinercionnyj ul'trafioletovyj vlagomer. *Izv. AN SSSR, Fiz. Atm. I okeana* **9**, 642-645.
- Lee, X., Massman, W. J., Law, B. (Editors), 2004: *Handbook of Micrometeorology: A Guide for Surface Flux Measurement and Analysis*. Kluwer, Dordrecht, 250 pp.

- Liebenthal, C., Foken, T., 2004: On the significance of the Webb correction to fluxes, Corrigendum. *Boundary-Layer Meteorol.* **113**, 301.
- Liebenthal, C., Foken, T., 2003. On the significance of the Webb correction to fluxes. *Boundary-Layer Meteorol.* **109**, 99-106.
- Lind, R. W. and Shaw W. J., 1991: The time-varying calibration of an airborne Lyman-alpha hygrometer. *J. Atmos. Oceanic Technol.* **8**, 186-190.
- Martini, L., Stark, B., Hunsalz, G., 1973: Elektronisches Lyman-Alpha-Feuchtemessgerät. *Z. Meteorol.* **23**, 207-209.
- Mauder, M. and Foken, T., 2004. Documentation and instruction manual of the eddy covariance software package TK2, *Arbeitsergebnisse, Universität Bayreuth, Abt. Mikrometeorologie. Print, ISSN 1614-8916*, 26, 42 pp.
- Moore, C. J., 1986: Frequency response corrections for eddy correlation systems. *Boundary Layer Meteorology* **37**: 17-35
- Ohtaki, E. and Matsui T., 1982: Infrared Device for Simultaneous Measurement of Fluctuations of Atmospheric Carbon Dioxide and Water Vapor. *Boundary Layer Meteorology* **24**, 109-119.
- Oncley, S. P., Foken, T., Vogt, R., Bernhofer, C., Kohsiek, W., Liu, H., Pitacco, A., Grantz, D., Ribeiro, L., Weidinger, T., 2002: *The energy balance experiment EBEX-2000. 15th Symp. on Boundary Layer and Turbulence, Wageningen, NL, 15-19 July 2002, Am. Meteorol. Soc.*, 1-4.
- Schotanus, P., Nieuwstadt, F. T. M., DeBruin, H. A. R., 1983: Temperature measurement with a sonic anemometer and its application to heat and moisture fluctuations. *Boundary Layer Meteorology* **26**: 81-93
- Thomas, C. and Foken, T., 2002: Re-evaluation of integral turbulence characteristics and their parameterization. *15th Conference on Turbulence and Boundary Layers, Wageningen, NL, 15-19 July 2002, Am. Meteorol. Soc.*, 129-132.
- Webb, E. K., Pearman, G. I., Leuning, R., 1980: Correction of the flux measurements for density effects due to heat and water vapour transfer. *Quart J Roy Meteorol Soc* **106**: 85-100.

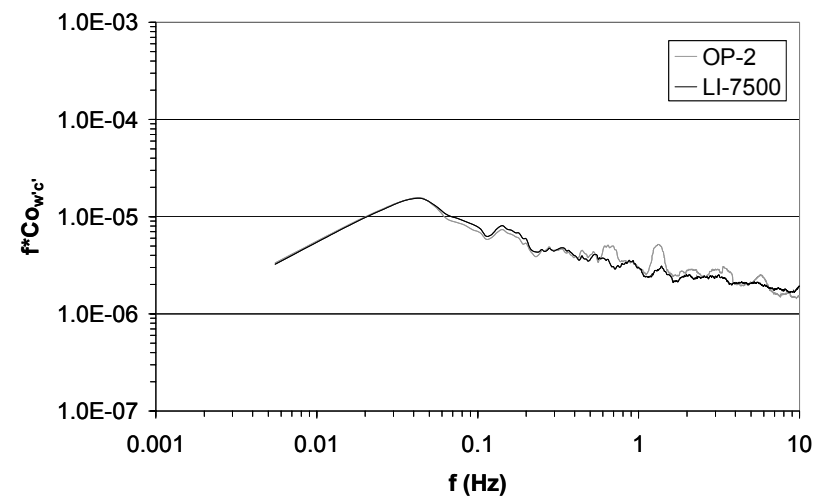
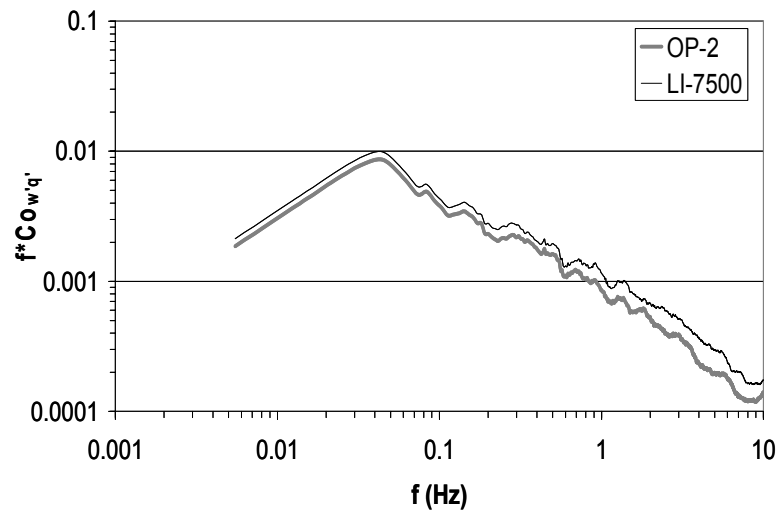
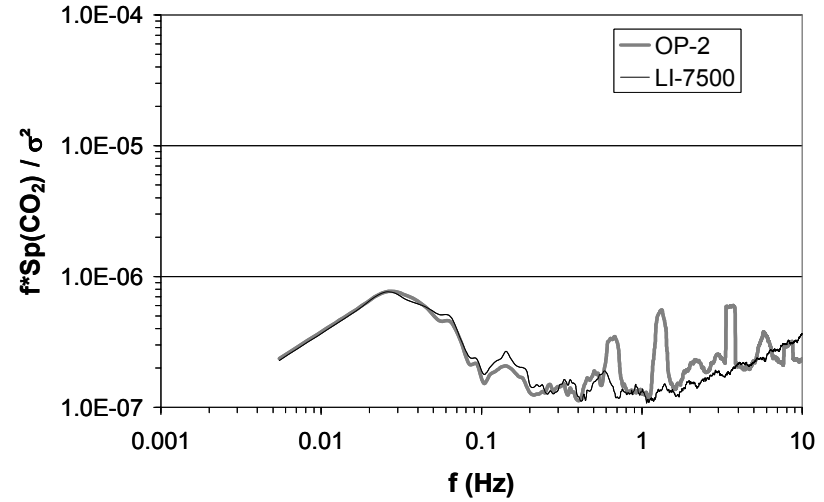
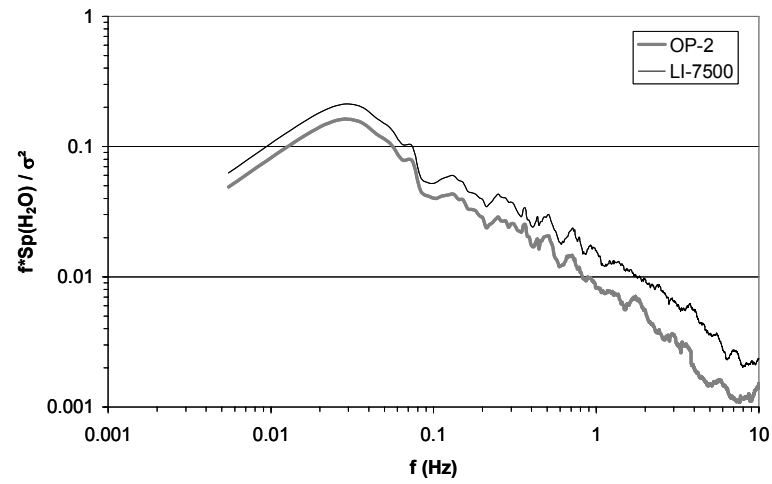
Appendix I



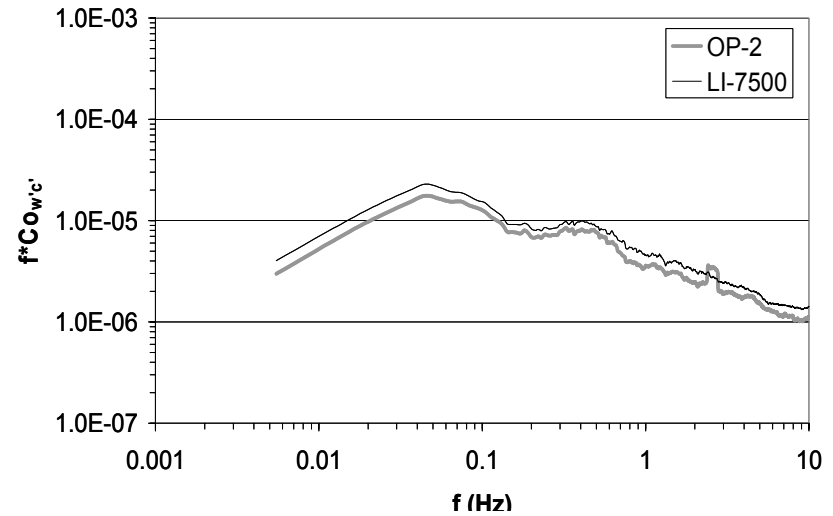
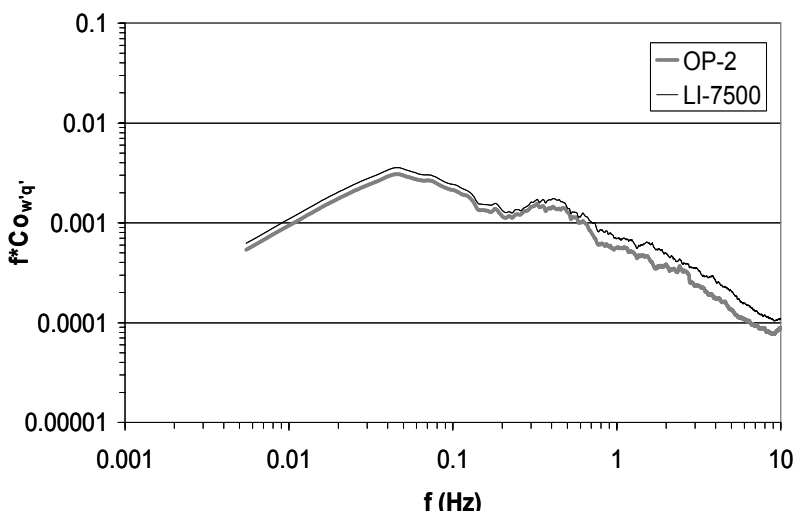
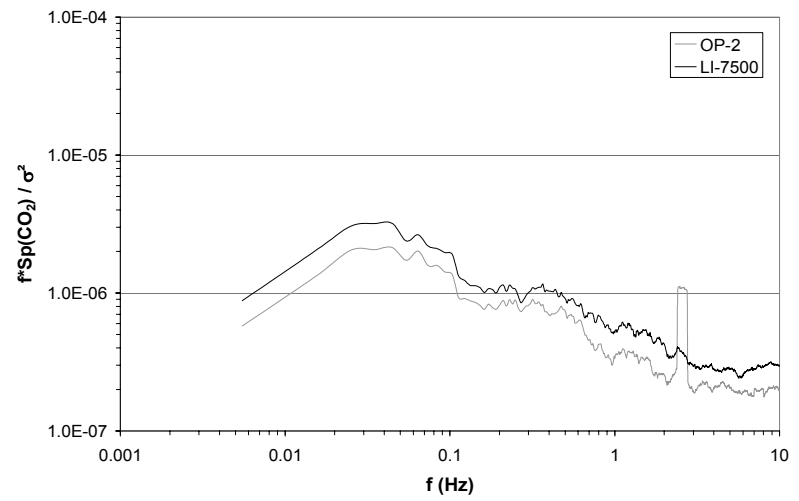
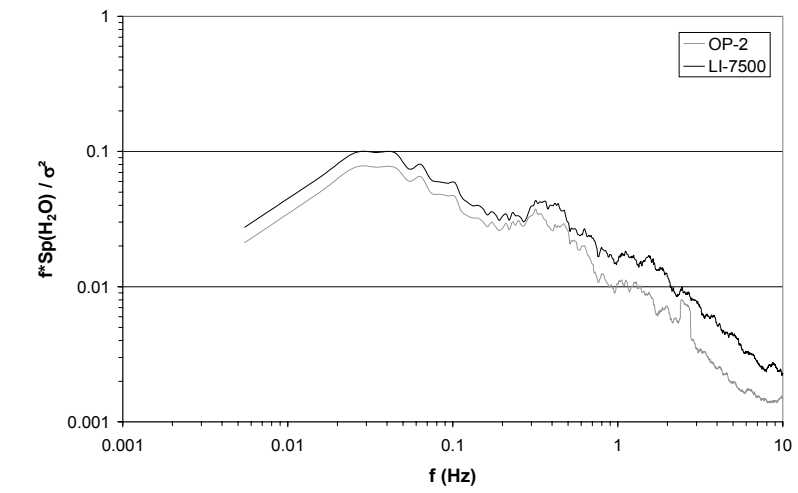
Annex I- 1: Power spectra (at the top) and cospectra (at the bottom) of water vapour (left side) and CO_2 (right side) July 7th, 2004, 00:30h.



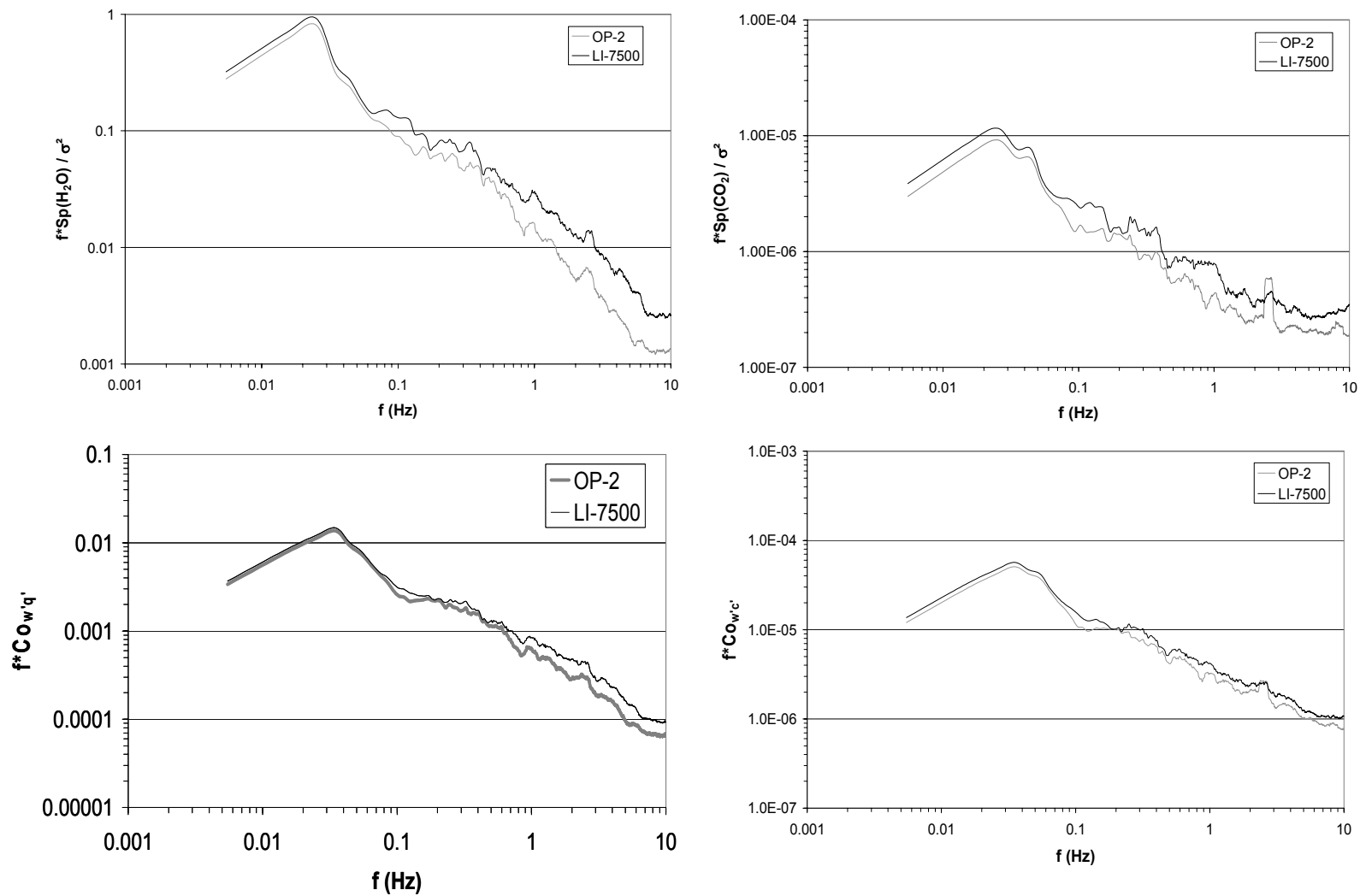
Annex I- 2: Power spectra of water vapour (left side) and CO₂ (right side) July 7th, 2004, 07:00h.



Annex I- 3: Power spectra (at the top) and cospetra (at the bottom) of water vapour (left side) and CO₂ (right side) July 7th, 2004, 15:30h.



Annex I- 4: Power spectra (at the top) and cospectra (at the bottom) of water vapour (left side) and CO₂ (right side) July 28th, 2004, 20:30h. The day was cloudy.



Annex I- 5: Power spectra (at the top) and cospectra (at the bottom) of water vapour (left side) and CO₂ (right side) July 30th, 2004, 09:00h.

Previously released papers in the series 'Universität Bayreuth, Abt. Mikrometeorologie, Arbeitsergebnisse' (University of Bayreuth, Department of Micrometeorology, Proceedings)

Nr	Name	Titel	Datum
01	Foken	Der Bayreuther Turbulenzknecht	01/99
02	Foken	Methode zur Bestimmung der trockenen Deposition von Bor	02/99
03	Liu	Error analysis of the modified Bowen ratio method	02/99
04	Foken et al.	Nachtfrostgefährdung des ÖBG	03/99
05	Hierteis	Dokumentation des Experimentes Dlouha Louka	03/99
06	Mangold	Dokumentation des Experiments am Standort Weidenbrunnen, Juli/August 1998	07/99
07	Heinz, Handorf, Foken	Strukturanalyse der atmosphärischen Turbulenz mittels Wavelet-Verfahren zur Bestimmung von Austauschprozessen über dem antarktischen Schelfeis	07/99
08	Foken	Comparison of the sonic anemometer Young Model 81000 during VOITEX-99	10/99
09	Foken et al.	Lufthygienisch-Bioklimatische Kennzeichnung des oberen Egertales, Zwischenbericht 1999	11/99
10	Sodemann	Stationsdatenbank zum BStMLU-Projekt Lufthygienisch-Bioklimatische Kennzeichnung des oberen Egertales	03/00
11	Neuner	Dokumentation zur Erstellung der meteorologischen Eingabedateien für das Modell BEKLIMA	10/00
12	Foken et al.	Dokumentation des Experimentes VOITEX-99	12/00
13	Bruckmeier et al.	Documentation of the experiment EBEX-2000, July 20 to August 24, 2000	01/01
14	Foken et al.	Lufthygienisch-Bioklimatische Kennzeichnung des oberen Egertales	02/01
15	Göckede	Die Verwendung des footprint-Modells nach SCHMID (1997) zur stabilitätsabhängigen Bestimmung der Rauigkeitslänge	03/01

16	Neuner	Berechnung der Evapotranspiration im ÖBG (Universität Bayreuth) mit dem SVAT-Modell BEKLIMA	05/01
17	Sodemann	Dokumentation der Software zur Bearbeitung der FINTUREX-Daten	08/02
18	Göckede et al.	Dokumentation des Experiments STINHO-1	08/02
19	Göckede et al.	Dokumentation des Experiments STINHO-2	12/02
20	Göckede et al.	Characterisation of a complex measuring site for flux measurements	12/02
21	Liebenthal	Strahlungsmessgerätevergleich während des Experimentes STINHO_1	01/03
22	Mauder et al.	Dokumentation des Experimentes EVA_GRIPS	03/03
23	Mauder et al.	Dokumentation des Experimentes Litfass-2003 Dokumentation des Experimentes GRASTATEM-2003	12/03
24	Thomas et al.	Documentation of WALDATEM-2003 Experiment	05/04
25	Göckede et al.	Qualitätsbegutachtung komplexer mikrometeorologischer Messstationen im Rahmen des VERTIKO-Projekts	11/04
26	Mauder und Foken	Documentation and Instruction Manual of the Eddy Covariance Software Package TK2	12/04
27	Herold G. et al.	The OP-2 open path infrared gas analyser for CO ₂ and H ₂ O	01/05